Dryopithecine palaeobiodiversity in the Iberian Miocene revisited on the basis of molar endostructural morphology

Clément Zanolli, Josep Fortuny, Federico Bernardini, Claudio Tuniz, David M Alba

Dryopithecine palaeobiodiversity in the Iberian Miocene revisited on the basis of molar endostructural morphology

Josep Fortuny[1,*] , Clément Zanolli[2] , Federico Bernardini[3,4] , Claudio Tuniz[3,4,5], David M. Alba[1,*]

[1]Institut Català de Paleontologia Miquel Crusafont, Universitat Autònoma de Barcelona, Edifici ICTA-ICP, c/ Columnes s/n, Campus de la UAB, 08193 Cerdanyola del Vallès, Barcelona, Spain; josep.fortuny@icp.cat, david.alba@icp.cat
[2]Université de Bordeaux, CNRS, MCC, PACEA, UMR 5199, 33600 Pessac, France; clement.zanolli@gmail.com
[3]Department of Humanistic Studies, Università Ca'Foscari, Venezia, Italy
[4]Multidisciplinary Laboratory, 'Abdus Salam' International Centre for Theoretical Physics, Via Beirut 31, 34151 Trieste, Italy; fbernard@ictp.it, ctuniz@ictp.it
[5]Center for Archaeological Science, University of Wollongong, Northfields Ave, Wollongong, NSW 2522, Australia

*Corresponding authors

Abstract: Extensive fieldwork at Abocador de Can Mata (north-east Iberian Peninsula) has uncovered a previously unsuspected diversity of catarrhine primates in the middle Miocene (12.5–11.6 Ma) of Europe. However, the distinction of the great ape genera *Pierolapithecus* and *Anoiapithecus* from *Dryopithecus* (supported by craniodental differences) has been disputed by some authors. Here we revisit the diversity of great apes (dryopithecines) from the Iberian Miocene based on molar 3D endostructural morphology (relative enamel thickness, enamel distribution, and enamel– dentine junction (EDJ)). Using microtomography, we inspected an extensive sample of 49 hominoid molars representing at least five species from 12 localities. 2D and 3D relative enamel thickness values indicate that *Dryopithecus* and '*Sivapithecus' occidentalis* (species inquirenda) display the thinnest and thickest enamel, respectively, while the remaining taxa (*Hispanopithecus*, *Anoiapithecus*, *Pierolapithecus*) show intermediate values. Upper molar enamel distribution maps exhibit a similar pattern in *P. catalaunicus*, *A. brevirostris*, *D. fontani*, *H. laietanus* and *H. crusafonti* whereas for the lower molars they reveal differences between *H. laietanus* and *H. crusafonti*. Lower molar enamel distribution and EDJ morphology of *'S.' occidentalis* support the distinction of this species but do not resolve whether it is a junior synonym of *Anoiapithecus* brevirostris or *Pierolapithecus* catalaunicus. Overall our results support the distinction of middle Miocene dryopithecins from late Miocene hispanopithecins, the distinction of *Pierolapithecus* and *Anoiapithecus* from *Dryopithecus* among the former, and the distinct species status of *H. crusafonti* compared to *H. laietanus* among the latter. Our results highlight the potential of inner tooth morphology for hominoid alpha-taxonomy.

Key words: fossil primates, Hominoidea, Dryopithecinae, dental morphology, enamel–dentine junction, relative enamel thickness.

The Miocene record of great apes (Primates, Hominidae) in the Iberian Peninsula is restricted to Catalonia in northeast Spain (Valles-Penedes and Seu d'Urgell basins) (Casanovas- Vilar et al. 2011; Alba 2012). Until two decades ago, all great apes from the Iberian Miocene were subsumed into a single genus, *Dryopithecus* (e.g. Begun et al. 1990; Harrison 1991; Begun 1992, 2002, 2007; Moyà-Solà & Kohler 1993, 1995; Ribot et al. 1996) although most of the available sample consisted of late Miocene remains (Golpe Posse 1993). Since 2002, new discoveries at the middle to upper Miocene Abocador de Can Mata (ACM) composite section (c. 12.6–11.4 Ma) (Alba et al. 2006, 2017; Casanovas- Vilar et al. 2011, 2016) have unveiled a previously unsuspected diversity of catarrhine primates (Alba 2012; Alba et al. 2017), including pliopithecoids (Alba et al. 2010a, 2012a), the small-bodied putative stem hominoid Pliobates (Alba et al. 2015), and as many as three great ape (hominid) genera, each represented by a single species: *Pierolapithecus* catalaunicus (Moyà-Solà et al. 2004); *Anoiapithecus* brevirostris (Moyà-Solà et al. 2009a; Alba et al. 2013); and *Dryopithecus* fontani (Moyà-Solà et al. 2009b; Alba & Moyà-Solà 2012). The former two of these were originally described based on ACM material (Moyà-Solà et al. 2004, 2009a). An isolated upper molar from els Hostalets de Pierola assigned to *Dryopithecus* by van der Made & Ribot (1999) most likely comes from levels younger than those recorded at ACM (Alba et al. 2013). Although this specimen was left unassigned to genus in some previous publications (e.g. Alba 2012; Alba et al. 2013), it is here attributed to *D. fontani* following Alba et al. (2020). In turn, a mandibular fragment from ACM is provisionally assigned to '*Sivapithecus' occidentalis* (Alba et al. 2020). This nominal species is currently recognized as a species inquirenda because, although it differs from D. fontani, additional material would be

required to discount an attribution to either *P. catalaunicus* or *A. brevirostris* (Alba et al. 2020). The recovery of cranial remains assigned to *Dryopithecus* at ACM also prompted the resurrection of genus *Hispanopithecus* (Moyà-Solà et al. 2009b) and the transferal into it of two late Miocene great ape species from the Valles-Penedes Basin *(H. laietanus* and *H. crusafonti*; see Begun 1992, 2002; Moyà-Solà & Kohler 1993, 1995; Golpe Posse 1993; Alba et al. 2012b) formerly assigned to *Dryopithecus* (see references above). All these genera are generally considered to belong to a single group, here distinguished as the subfamily Dryopithecinae (Alba 2012), whose phylogenetic affinities are still unclear, being generally considered to be either stem hominids (Moyà-Solà et al. 2004, 2009a; Alba 2012; Alba et al. 2015) or hominines (Begun 2009, 2015; Begun et al. 2012). The distinction of two species of *Hispanopithecus* (Begun 1992; Cameron 1999; Alba et al. 2012b), formerly criticized by several authors (Harrison 1991; Andrews et al. 1996; Ribot et al. 1996), also relies on dental differences and therefore requires more detailed studies. While the distinction of *Hispanopithecus* is currently universally accepted (Casanovas-Vilar et al. 2011; Alba 2012; Begun et al. 2012; Alba et al. 2012b, 2015; Begun 2015; Bohme et al. 2019), the recognition of three middle Miocene dryopithecine genera in the Valles-Penedes Basin (Casanovas-Vilar et al. 2011; Alba 2012; Alba & Moyà-Solà 2012; Alba et al. 2013, 2020; Perez de los Rıos et al. 2013; Marigo et al. 2014) has been accepted by some (Pickford 2012; Fleagle 2013; Bohme et al. 2019; Andrews 2020) but questioned by others (Begun 2009, 2010, 2015). In particular, both *Pierolapithecus* and *Anoiapithecus* have been considered likely junior synonyms of *Dryopithecus* (Begun 2009). Although the distinction of the former is mainly based on cranial anatomy (Moyà-Solà et al. 2004, 2009a, b; Alba 2012; Perez de los Rıos et al. 2012) subtle differences in dental morphology have also been argued to differentiate these two genera from one another, and relative to both *Dryopithecus* and *Hispanopithecus* (Alba & Moyà-Solà 2012; Alba et al. 2013, 2020; Perez de los Rıos et al. 2013). Although the postcranial record is more restricted (unknown for *Anoiapithecus*) it also supports the genus distinction between *Pierolapithecus* and *Hispanopithecus* (Moyà-Solà et al. 2004, 2005; Almecija et al. 2007, 2009; Alba et al. 2010c, 2011, 2012c) and hints at some differences between *Dryopithecus* and the two former genera (Moyà-Solà et al. 2009b; Almecija et al. 2013; Pina et al. 2012, 2019). Enamel thickness variation (Alba et al. 2010b, 2013, 2020) and, most recently, crown endostructural variation (Alba et al. 2020) have also been investigated to clarify the allocation of fragmentary dentognathic remains (Alba et al. 2020). A large proportion of hominoid specimens from the Valles-Penedes Basin are fragmentary denthognatic remains or isolated teeth. Therefore, dental morphology plays a very important role in the alphataxonomy of these taxa. Unfortunately, taxonomic assessments based on the dental morphology of Iberian dryopithecines are complicated by small sample sizes and overall similarities in occlusal morphology. Non-invasive techniques based on x-ray microcomputed tomography (μCT) provide a wealth of additional information on the inner structural morphology of teeth (Macchiarelli et al. 2013), which complements and augments that provided by the outer enamel surface (OES). The latter is often affected by occlusal wear or taphonomic damage. In contrast, μCT grants non-destructive access to tooth endostructural morphology and enables the assessment of taxonomic and functionally-related parameters such as enamel thickness distribution over the crown, as well as enamel–dentine junction (EDJ) shape. To test the hypothesis that the Iberian Miocene hominid diversity includes at least four genera (*Pierolapithecus*, *Anoiapithecus*, *Dryopithecus*, *Hispanopithecus*)

and further evaluate the taxonomic distinctiveness of these Miocene dryopithecines from Catalonia, we investigate the internal dental morphology based on most of the available upper and lower molars. Enamel thickness, previously investigated for the middle Miocene (Alba et al. 2010b, 2013, 2020) and late Miocene (Andrews & Martin 1991; Smith et al. 2019) dryopithecines, is here analysed in 2D and, for the first time, in 3D. We also describe the EDJ morphology of these taxa in relation to previous observations based on OES morphology, and based on these data we re-evaluate the distinction between the investigated dryopithecine taxa. Based on the previously published research cited above, differences in terms of dental endostructural organization are to be expected between: (1) middle Miocene and late Miocene hominoids; (2) *Dryopithecus* as compared to *Pierolapithecus* and *Anoiapithecus* (and '*S.*' *occidentalis*), particularly in terms of tissue proportions; and (3) *H. crusafonti* and *H. laietanus*, with the latter being somewhat more derived relative to the middle Miocene genera.

Material and Method

Dental terminology The dental terminology employed in the descriptions is depicted in Fortuny et al. (2021, SI fig. 1). It follows that of Harrison & Gu (1999), except that 'protoconule' is favoured over 'paraconule' (Swindler 2002). Upper molar positions are indicated with superscript numbers (e.g. M1) and those of lower molars with subscript (e.g. M2). Studied sample Our sample consists of 49 (30 upper and 19 lower) permanent molars from 25 specimens representing a minimum of 15 individuals from 12 localities (see Table 1 for provenance details). The specimens are housed at the Institut Català de Paleontologia Miquel Crusafont, Sabadell, Spain (IPS), except for two specimens housed at the Museu de Geologia del Seminari de Barcelona, Spain (MGSB). Computational techniques Microcomputed tomography acquisitions. Specimens were imaged by microfocus x-ray microcomputed tomography (μCT) at the Multidisciplinary Laboratory of the 'Abdus Salam' International Centre for Theoretical Physics of Trieste. The scans were made with a transportable scanner specifically designed for the investigation of cultural heritage items. X-rays are produced by a Hamamatsu microfocus x-ray source (150 kV maximum voltage, 500 mA maximum current, and 5 mm minimum focal spot size) and the detector is a Hamamatsu CMOS flat panel coupled to a fibre optic plate under the GOS scintillator. The system has been designed to allow large sample-to-detector distances to exploit phase-contrast effects (Tuniz et al. 2013). The acquisitions were performed according to the following parameters: 120–150 kV voltage; 62–201 lA current; a projection each 0.15°–0.20° (see Fortuny et al. 2021, table 1 for details). Virtual reconstruction and segmentation. The final volumes were reconstructed using Cobra v.7.4.16 (Exxim) and DigiCT v.2.3.3 (DIGISENS) in 8-bit format, with an isotropic voxel size ranging from 14.36 to 20.42 lm (see Fortuny et al. 2021, table 1 for details). Using Avizo 7.0 (FEI-Visualization Sciences Group Inc.) and ImageJ v.1.47 (NIH; Schneider et al. 2012), a semiautomatic threshold-based segmentation was carried out (Fortuny et al. 2021, SI fig. 2) following the half-maximum height method (HMH; Spoor et al. 1993) and the region of interest thresholding protocol (ROI-Tb; Fajardo et al. 2002), taking repeated measurements on different slices of the virtual stack (Coleman & Colbert 2007). Digital surface models of the OES and EDJ of the investigated molars are available on MorphoSource (Fortuny 2021). OES models are openly shared from MorphoSource, whereas the EDJ are

available on request; see Fortuny et al. (2021, table 2) for digital object identifiers and further details. Relative enamel thickness. 2D relative enamel thickness (RET) was computed following a protocol originally devised for histological sections (Martin 1985). In order not to overestimate RET due to obliquity, it was assessed on virtual coronal buccolingual sections perpendicular to the best-fit plane of the cervical line and passing through the tips of the mesial dentine horns (Benazzi et al. 2014). This method has previously been used to compute 2D RET values for the middle Miocene specimens included in this study (Alba et al. 2013, 2020). The following formula was employed (Martin 1985; Smith et al. 2005; Alba et al. 2010b): 2D RET = 2D AET 9 100/b1/2, wherein b is the dentine and pulp area, 2D AET is average enamel thickness, computed as 2D AET = c (enamel cap area)/ e (enamel–dentine junction length). While 2D RET is a dimensionless variable originally developed to compare enamel thickness among species of different tooth size (Martin 1985), the assessment of intra-individual intertooth variation should instead be based on 2D AET (Smith et al. 2005). Following previous studies (e.g. Smith et al. 2005), for several specimens it was necessary to correct RET calculations for tooth wear. As frequently done to maximize the sample available for the estimation of tissue proportions (e.g. Smith et al. 2006, 2012a; Martin-Francés et al. 2018), reconstructions of the worn enamel and dentine horn tip were made prior to measurement for sections showing light to moderate wear, or when a small amount of cervical enamel was missing (based on the curvature and orientation of the outer enamel surface relative to the EDJ). Tooth wear stages were assessed following the adaptation of a previous protocol established on human teeth (Smith 1984). Specimens that were too heavily worn (above stage 4) were excluded. In consequence, a total of 41 specimens (25 upper molars and 16 lower molars) were analysed for 2D RET. The formulae employed to compute 3D AET and 3D RET are three-dimensional extensions of those employed to compute 2D RET (Olejniczak 2006; Olejniczak et al. 2008a, b, c, d; Benazzi et al. 2014): 3D AET = Ve/SEDJ and 3D RET = 3D AET 9 100/Vcdp1/3, wherein Ve is enamel cap volume, Vcdp is dentine and pulp volume, and SEDJ is EDJ surface area. A total of 31 specimens (21 upper molars and 10 lower molars) were analysed for 3D RET. We refrained from using discrete categorizations of enamel thickness stemming from the thin versus thick dichotomy (Martin 1985), because they do not adequately reflect either the continuum displayed among different teeth of a single individual or intraspecific and interpecific variability. Therefore, comparisons between the analysed Miocene apes and other hominoids were based on statistical comparisons of 2D RET and 3D RET values among species. For 2D RET results we also included in the statistical comparisons the data derived from the histological sections used by Andrews & Martin (1991) and Kelley et al. (2001) as reported by Smith et al. (2019). The small available sample sizes precluded performing statistical tests to assess differences in RET for different tooth loci separately, as such comparisons would not have enough statistical power to distinguish significant differences. Statistical comparisons were instead done by lumping the data from all tooth loci. These comparisons should be taken with great care because there is a trend towards increasing relative enamel thickness from the first to third molars in both humans and apes (Grine & Martin 1988; Macho 1994; Grine 2002, 2005; Smith et al. 2005, 2006, 2019). To account for this problem, we compared individual data for Valles-Penedes hominoids with the median values and range of variation displayed by extant great ape genera for each tooth locus separately (Smith et al. 2008, 2012b, 2019). Comparisons of 2D RET and 3D RET values for both extant and

extinct taxa were made with PAST v. 4.01 (Hammer et al. 2001) by means of Kruskal–Wallis tests for equality of medians and pairwise Mann–Whitney post hoc comparisons, which are non-parametric and hence do not assume normal distributions, with and without Bonferroni correction. Adjusted z-score analyses were performed for 2D RET and 3D RET from the Iberian Miocene great apes and on five extant comparative taxa. This method allows the comparison of unbalanced samples, which is often relevant in the fossil record. Enamel distribution maps. Enamel distribution maps permit comparisons in the local distribution of enamel over the entire crown surface (Macchiarelli et al. 2008, 2009, 2013; Zanolli et al. 2019; Thiery et al. 2017). Enamel thickness topographic variation was rendered for 44 specimens (25 upper molars and 19 lower molars) using 3D cartographies and a chromatic scale in which thickness increases from dark blue (thin) to red (thick) (Macchiarelli et al. 2008, 2013; Bayle et al. 2011). The software Avizo 7.0 (FEI-Visualization Sciences Group Inc.) was used for this purpose. This visualization technique maps the local enamel thickness by computing the site-specific shortest distance between the OES and EDJ surfaces. EDJ morphology. The morphology of the EDJ was examined in the same 44 specimens. The Miocene hominid molars exhibit expression of non-metric features that are not covered with the usual scoring systems, such as the Arizona State University Dental Anthropology method that was developed for human/hominin teeth (Turner et al. 1991; Scott & Irish 2017). Therefore, we elaborated a qualitative approach based on a limited number of stages for each feature.

Results

Enamel thickness 2D RET was computed for 41 specimens (see Fortuny et al. 2021, table 3, and sections used in Fortuny et al. 2021, SI figs 3–5). 2D RET values for 20 specimens, attributed to *P. catalaunicus*, *A. brevirostris*, *D. fontani* and 'S' occidentalis, have been published previously (see Alba et al. 2013, 2020), while 3D RET is newly reported for 31 specimens (see Fortuny et al. 2021). Based on average 2D RET values (Table 2; Fig. 1A; see Fortuny et al. 2021, table 5, SI figs 6, 7A), *D. fontani* displays the thinnest enamel (12.3 μm), while *'S.' occidentalis* displays the thickest (19.7 μm) in this sample, with other dryopithecines having similar intermediate average values; in order of increasing 2D RET: *H. laietanus* (14.3 μm), *H. crusafonti* (14.4 μm), *A. brevirostris* (14.6 μm) and *P. catalaunicus* (15.4 μm). Such apparent differences in average RET values among these taxa cannot be taken at face value and must be interpreted with great care, given the small samples available for most of the taxa and the variation displayed by extant taxa; this is further illustrated by the range of *H. laietanus* (10.3– 19.1 μm, N = 17), which broadly overlaps the values for the remaining taxa. Our results for average 3D RET (Table 2; Fig. 1B; see Fortuny et al. 2021, table 5, SI fig. 7B) also indicate that *D. fontani* (11.9 μm) and *'S.' occidentalis* (19.0 μm) display the thinnest and thickest enamel, respectively, with the remaining taxa showing intermediate average values; in order of increasing 3D RET: *H. crusafonti* (12.1 μm), *A. brevirostris* (12.9 μm), *H. laietanus* (13.5 μm) and *P. catalaunicus* (15.5 μm). Although the *'S.' occidentalis* sample displays the thickest enamel, it should be taken into account that this result is likely to be biased by small sample size coupled with the lack of first molars available for analysis. Statistical comparisons based on Kruskal–Wallis tests for equality of medians show significant differences among extant apes in both 2D RET ($v2 = 38.31$, $p < 0.001$) and 3D RET

(v2 = 32.05, p < 0.001). Mann– Whitney pairwise comparisons in 2D and 3D RET (See Fortuny et al. 2021, table 6) indicate that African apes (Gorilla and Pan) and siamangs display similarly thin enamel, whereas orangutans and gibbons display significantly thicker enamel (see average and maximum–minimum values in Fortuny et al. 2021, tables 7, 8). Chimpanzees display slightly thicker enamel than gorillas only for 3D RET, whereas differences in 2D RET become nonsignificant after Bonferroni correction, and the same occurs between siamangs and gibbons. Comparisons between the fossil samples and extant taxa are possible for both 2D and 3D RET (Fortuny et al. 2021, tables 7 and 8, respectively), but comparisons with other extinct taxa are mostly restricted to 2D RET due to the lack of 3D data (with only two exceptions; see Fortuny et al. 2021, table 8). We therefore compared 2D RET among Iberian dryopithecines, extant hominoids, and two fossil hominoid samples (the kenyapithecine *Griphopithecus* and the dryopithecine *Rudapithecus*; see descriptive statistics in Fortuny et al. 2021, table 9, SI fig. 7A) whereas comparisons for 3D RET were restricted to Iberian dryopithecines and extant taxa (see Fortuny et al. 2021, table 10, SI fig. 7B). When these enlarged samples are considered, Kruskal–Wallis tests show again significant differences in both 2D RET (v2 = 23.44, p < 0.001) and 3D RET (v2 = 13.84, p < 0.001). Mann–Whitney pairwise comparisons are reported for fossil taxa as compared with the extant hominoid samples discussed above (see Fortuny et al. 2021, table 11). Based on the currently available, restricted fossil samples, 2D RET comparisons indicate that all extinct taxa show thicker enamel than gorillas and chimpanzees, and most also display thicker enamel than siamangs, with the exception of *D. fontani* (although differences also approach the p = 0.05 significance threshold, for *H. laietanus* and *Rudapithecus*). In contrast, most extinct taxa display lower 2D RET than Pongo, except *Griphopithecus*, *P. catalaunicus* and *'S.' occidentalis*, which do not differ from orangutans. However, like most other extinct taxa, *P. catalaunicus* does not differ from gibbons, whereas *Griphopithecus* and *'S.' occidentalis* show instead thicker enamel (although the *'S.' occidentalis* sample is biased, as explained above) (Fortuny et al. 2021, SI fig. 7A). Based on 3D RET, fewer significant differences are found, probably as a result of smaller sample sizes. Only *'S.' occidentalis* clearly shows thicker enamel than extant apes (although this is probably biased, see above), whereas *H. laietanus* and *A. brevirostris* display thicker enamel than siamangs and gorillas (although comparisons with chimpanzees only approach significance), while *P. catalaunicus* further displays thicker enamel than chimps, more closely resembling orangs and gibbons. Adjusted z-scores for 2D RET (see Fortuny et al. 2021, SI fig. 8A, table 12) and 3D RET (see Fortuny et al. 2021, SI fig. 8B, table 13) for each fossil specimen compared with extant hominoid samples may clarify the results provided above, especially for the smaller samples, as it is the case for *'S.' occidentalis* in both 2D RET and 3D RET, as well as *P. catalaunicus*, *H. crusafonti* and *D. fontani* in 3D RET. Due to the extensive overlap among extant taxa, particularly when all tooth loci are considered simultaneously, many specimens fit within the variation of all the comparative samples, although others do significantly differ from some. For all the taxa examined, some specimens differ from African apes and, for *H. laietanus*, *P. catalaunicus*, and *'S.' occidentalis*, also from siamangs, whereas most specimens do not differ from either gibbons or orangutans. In fact, in 2D, only a single specimen of *H. laietanus* and two of *'S.' occidentalis* show significantly thicker enamel than orangutans, whereas in 3D there is a single specimen of *'S.' occidentalis* that shows thicker enamel than both siamangs and humans. While the sample size of Miocene apes available for 3D estimates is

smaller than for 2D analyses, the results show high coherence. Enamel distribution maps Enamel distribution maps (Figs 2, 3) in *D. fontani* upper molars show that the thickest enamel is on the periphery of the cusps and marginal ridges, with much thinner enamel in the trigon than over the talon basin. The upper molars of *P. catalaunicus, A. brevirostris* and *H. laietanus* overall show a similar enamel distribution pattern to *D. fontani*, except that the enamel is relatively thicker on the trigon basin. A specimen of *H. laietanus* (IPS58340) somewhat differs by having its thickest enamel limited for the most part to the protocone, while both the trigon and talon basins display thinner enamel. In the upper molars of *H. crusafonti*, thicker enamel is distributed over the talon basin and lateral walls, although, with the exception of the protocone, the trigon enamel is moderately thin to thin. In the lower molars of *H. laietanus*, the thickest enamel is found on the periphery of the talonid, while the trigonid (even buccally) generally shows moderately thick enamel. The only exception is IPS1822 (the invalid holotype of '*D. piveteaui*', currently included in *H. laietanus*), which displays its thickest enamel only on the outer aspect of the buccal cusps, as in the paratype of *H. crusafonti* IPS1816. The molars of *H. crusafonti* MGSB25314 have in contrast their thickest enamel located on the outer aspect of the cusps, their inner aspects being also relatively thick (only the centre of the occlusal basin and the cervical part of the crown are thin enamelled). The holotype of *'S.' occidentalis*, in turn, displays a similar enamel distribution pattern as IPS1822 and IPS1816, with the thickest areas mostly located on the buccal half of the crown (notably on the outer aspect of the buccal cusps, up to the cusp apex), and thinner enamel being located lingually. '*Sivapithecus' occidentalis* IPS41734, although somewhat worn, also approximates the enamel distribution shown by IPS1822 and the holotype of *'S.' occidentalis*. EDJ morphology Outer enamel surface morphology (see Fortuny et al. (2021, SI figs 9, 10) of all the dryopithecine upper molars considered in this study displays a similar pattern, which is also reflected at the EDJ but with a sharper topography (Fig. 4; Table 3). All the M1s and M2s display four developed dentine horns at the EDJ, corresponding to the four main cusps visible on the OES (see Fortuny et al. 2021, SI fig. 9), whereas in the M3 one of the two distal cusps is frequently absent in accordance with their generally shorter and more distally-tapering crowns. Thus, no hypocone dentine horn is expressed in the M3 of *P. catalaunicus* (Fig. 4C), whereas it is well expressed *A. brevirostris* (Fig. 4J) and *H. crusafonti* (Fig. 4T, U), and discernible (if smaller) in *D. fontani* (Fig. 4G). In the M3 of *H. laietanus*, the hypocone is present, but the metacone horn is very poorly developed (Fig. 4X, Y), which contrasts with the distinct M3 metacone displayed by the other taxa (with the exception of one M3 of *H. crusafonti*; Fig. 4T). The dentine horns of the upper molar four main cusps are more centrally situated in *P. catalaunicus* and especially in *D. fontani* (Fig. 4D–G) than in *A. brevirostris, H. crusafonti* and especially *H. laietanus* (Fig. 4V–Y), which have more peripherally and vertically set dentine horns, in accordance with their less flaring crowns. In the M1s and M2s of *A. brevirostris* (Fig. 4H, I, M–P) and *H. crusafonti* (Fig. 4Q–S), the hypocone dentine horn is clearly more lingual than the protocone, as in the *D. fontani* M1 (Fig. 4E) but unlike in the remaining specimens. The mesial fovea, slit-like at the OES, appears as a larger, ovoid to subrectangular depression at EDJ level, even if much smaller than the trigon basin, particularly in the M3s. This fovea appears shallower and slightly more inclined mesialward in *P. catalaunicus* (Fig. 4A–C) and *D. fontani* (Fig. 4D–G) than in the remaining species, and also more mesially projected in the latter. In *A. brevirostris* (Fig. 4H–P) and especially *Hispanopithecus* spp. (Fig. 4Q–Y), the mesial fovea is mesiodistally shorter, more

buccally positioned, deeper, and enclosed by a stronger mesial marginal ridge. The mesial fovea is generally separated from the trigon basin by a well-developed hypoparacrista that links the paracone with the protoconule (except in a few specimens, e.g. Fig. 4U, V). The protoconule is often obliterated by wear on the OES, but a distinct dentine horn subequal in size to those of the four main cusps is frequently evidenced at the EDJ, even if variably developed: it is generally less developed in M3 (except in *P. catalaunicus*; Fig. 4C), and only poorly developed in the M2 of *D. fontani* MGSB48486 (Fig. 4D). The hypoparacrista generally terminates at the protoconule, but in some instances it joins the mesial marginal ridge, as in the M3s of *P. catalaunicus*, *D. fontani*, *A. brevirostris* and *H. crusafonti* (Fig. 4C, G, J, T), and some M2s of *A. brevirostris* (Fig. 4L) and *H. laietanus* (Fig. 4W). In the two latter taxa, a secondary small dentine horn is also present at the junction of the hypoparacrista with the marginal ridge. The hypoparacrista generally originates nearby the paracone dentine horn apex, although in the M3 of *D. fontani* and *A. brevirostris* (Fig. 4G, J) it originates more mesially. At the EDJ, the trigon basin displays a subrhomboid contour (instead of a triangular one, as in the OES) in all the taxa, but is shallower in *D. fontani* (Fig. 4D–G) and *H. laietanus* (Fig. 4V–Y). The crista obliqua is high, complete and generally straight in *P. catalaunicus* (Fig. 4A–C) and *A. brevirostris* (Fig. 4H–M), although it is somewhat discontinuous (Fig. 4N–O) or even poorly developed (Fig. 4P) is some molars of the latter species. In *D. fontani* (Fig. 4D–G), the crista obliqua is low and less straight, due to the slightly curved postprotocrista, resulting in a sinuous crista obliqua in one specimen (Fig. 4G). In *Hispanopithecus* spp. (Fig. 4Q–Y), the crista obliqua is even lower and more diffuse, particularly in *H. crusafonti* (Fig. 4Q–U), being interrupted (non-merging postprotocrista and hypometacrista) in the two M3s of *H. crusafonti* (Fig. 4T, U) and one of the M3s of *H. laietanus* (Fig. 4X). In all the taxa, the talon basin is subtriangular and smaller than the trigon basin, also being shallower than the latter in *P. catalaunicus* (Fig. 4A–C), *A. brevirostris* (Fig. 4H–P) and *H. crusafonti* (Fig. 4Q–U). In most specimens, the talon basin is divided by a transverse and low hypocone-metacone crista, more clearly discerned at the EDJ than at the OES. This crista is generally more distinct in the M1 than in the M2, and absent from the M3. When present, it delimits a distal fovea from the deeper and more expansive talon basin, originating from the hypocone dentine horn and joining the end of the postmetacrista (only with some exceptions; Fig. 4K, Q, V). The upper molars display a subquadrangular (M1) to subrectangular (M2) occlusal outline, except for the M3 of *P. catalaunicus*, *A. brevirostris* and *H. laietanus* (Fig. 4C, J, X, Y), which display an ovoid to subtriangular profile due to the truncated talon. The degree of talon development is quite variable in *Hispanopithecus*, as previously noted based on the OES (Alba et al. 2012b), encompassing differences among the other species in this regard. The degree of buccolingual waisting of the upper molars at EDJ level is more marked in *A. brevirostris* (Fig. 4H, I, K–P), slightly less developed in *D. fontani* (Fig. 4D–G), more variable in *H. crusafonti* and *H. laietanus* (Fig. 4Q– W), and least developed in *P. catalaunicus* (Fig. 4A, B). The weak to moderate development of the lingual cingulum at the OES is variably expressed at the EDJ, ranging from the lack of this feature to a shelf bordered by a (semi)continuous crest extending along the lingual aspect of the protocone, sometimes connecting the lingual groove separating the protocone and hypocone. Even if decreasing in expression from the M1 to the M3, the lingual cingulum tends to be more developed in *A. brevirostris* and *H. crusafonti* (Fig. 4H–U), only moderately expressed in *D. fontani* (Fig. 4D–G), and even less so in *P. catalaunicus* (Fig. 4A–C) and *H. laietanus* (Fig.

4V, W). A buccal cingular remnant (in the form of a short crest enclosing a small fovea) frequently appears at the external end of the buccal groove at the EDJ in the M1 and most M2 of *A. brevirostris* (Fig. 4H, K, L–P) and *H. crusafonti* (Fig. 4Q–S). Similarly, a shelf-like structure is visible at the same spot in some specimens of *D. fontani* (Fig. 4E, F) and the M1 of *P. catalaunicus* (Fig. 4A). In contrast, the buccal aspect is rather smooth in *H. laietanus* (Fig. 4V, W) and the remaining specimens of *P. catalaunicus* (Fig. 4B). The overall endostructural pattern of the lower molars (Fig. 5; Table 4) is similar to the OES morphology (see Fortuny et al. 2021, SI fig. 10), with five well-developed dentine horns corresponding to the five main cusps. The dentine horns are generally vertically set, with the exception of the metaconid dentine horn of *'S.' occidentalis* specimens (Fig. 5A–C), which is tilted toward the centre of the tooth. In some specimens of *Hispanopithecus* spp., the metaconid dentine horn is also somewhat centrally tilted (especially in the M3 of MGSB25314; Fig. 5J), although to a lesser extent. The lingual dentine horns are very peripherally situated relative to the crown margin, whereas those corresponding to protoconid and hypoconid are less peripheral. This is more clear-cut in *'S.' occidentalis* specimens (Fig. 5A–C) compared to *Hispanopithecus*, although this feature is variable within both *H. crusafonti* (Fig. 5G–J) and *H. laietanus* (Fig. 5K–S). At the OES, *H. laietanus* (see Fortuny et al. 2021, SI fig. 10K, N–S) displays a more reduced buccal cingulid than the remaining taxa (see Fortuny et al. 2021, SI fig. 10A–J), in which it is nevertheless discontinuous. This difference is more marked at the EDJ (Fig. 5), where the buccal cingulid becomes shelf-like (at least between protoconid–hypoconid and hypoconid–hypoconulid) except in *H. laietanus* (Fig. 5K, N–S), in which it is only minimally developed if at all. Buccolingual crown waisting is also more strongly expressed at the EDJ, being most marked in *H. laietanus* (Fig. 5K, N–S) both buccally and lingually, whereas in *'S.' occidentalis* (Fig. 5A–C) and *H. crusafonti* (Fig. 5G–J), waisting is moderate to slight. Some specimens express additional cuspulids at the EDJ level. While no tuberculum sextum (C6) is expressed in any specimen at either the OES or the EDJ level, the M2 of the *'S.' occidentalis* holotype (Fig. 5B) and an M2 of *H. crusafonti* (Fig. 5G) display a well-developed interconulid- type tuberculum intermedium (C7) at the distal end of the postmetacristid, which at the OES is merely expressed as a secondary (cuspulid-like) thickening of the enamel. Furthermore, the M2 of *'S.' occidentalis* specimens (Fig. 5A–C) display a mesiodistally-elongated metaconid dentine horn with a distinct tuberculum intermedium or metaconulid-type C7 horn just distally from the main metaconid dentine horn. This 'twinned' metaconid morphology, also expressed at the OES as a cuspulid-like enamel thickening, is lacking in *H. crusafonti* (Fig. 5G–J), but variably expressed (although to a lesser extent) in most lower molars of *H. laietanus* (Fig. 5K, N–S), sometimes being discernible at the OES (see Fortuny et al. 2021, SI fig. 10K, L, N, O, R). The mesial fovea is much shorter mesiodistally than buccolingually broad and not completely isolated from the much deeper and more extensive talonid basin, since the hypoprotocristid and hypometacristid junction is interrupted by a mesiodistal fissure. These cristids, less discernible at the EDJ than the OES, are less marked in *Hispanopithecus* spp. (Fig. 5G–S) than in the remaining taxa (Fig. 5A–C). At the EDJ, the cristid obliqua is generally more distinct than at the OES, although it is also incomplete (the postprotocristid and prehypocristid junction is interrupted, although the buccolingual groove present at the OES is not discernible at the EDJ). Similarly, the profuse development of secondary enamel wrinkling on the talonid basin displayed by some specimens (*'S.' occidentalis*

and *H. laietanus*; see Fortuny et al. 2021, SI fig. 10B, C, S) has no concomitant expression at the EDJ. Only the obliquely-oriented crest (postcristid + hypoentocristid) separating the talonid basin from the more restricted distal fovea at the OES of most specimens (even if partially interrupted by a mesiodistal groove; see Fortuny et al. 2021, SI fig. 10) can generally be discerned at the EDJ. However, on the latter it is variably expressed, ranging from a continuous but low crest in most specimens, to a poorly expressed or even indistinguishable structure in some M2s (Fig. 5I, O, Q) and M3s (Fig. 5C, R, S).

Discussion

Our results allow us to refine these previously-reported differences in RET and dental morphology among middle Miocene hominoids from Catalonia (Alba & Moyà-Solà 2012; Alba et al. 2010b, 2013, 2020; Perez de los Rıos et al. 2013) and further provide additional information regarding the distinction between the late Miocene species *H. laietanus* and *H. crusafonti* (Begun 1992; Cameron 1999; Alba et al. 2012b). Enamel thickness This study extends the previously published results of 2D RET for middle Miocene dryopithecines from Catalonia (Alba et al. 2013, 2020) to *Hispanopithecus*, for which only limited evidence was available in the case of *H. laietanus*, based on a few histological sections (Andrews & Martin 1991; Kelley et al. 2001; Smith et al. 2019). Most importantly, however, we report 3D RET results for all these taxa for the first time. The enamel of *A. brevirostris* was originally reported as similarly thick to that of *P. catalaunicus* (Moyà-Solà et al. 2009b; Alba et al. 2010b), and both were assessed as considerably thicker-enamelled than *D. fontani* (Alba et al. 2010b), thereby contradicting the previous contention that all the middle Miocene dryopithecines from Catalonia were thin-enamelled (Begun 2009) as well as the purported synonymy of the former with *D. fontani* (Begun 2007, 2009). The significance of such differences has been disputed on the basis that enamel thickness is too variable among extant and extinct hominoids to be reliable as a taxonomic criterion (Begun et al. 2012). Such differences were subsequently confirmed to some extent using slightly enlarged samples for *A. brevirostris* and *D. fontani* and based on higher resolution scans (the same used in this paper; Alba et al. 2013, 2020). However, the latter studies showed that both *A. brevirostris* and *P. catalaunicus* display thinner enamel than originally reported (Alba et al. 2010b), being more similar to extant orangutans, albeit still significantly thicker than *D. fontani*, most similar to extant African apes (Alba et al. 2013, 2020). Caution is required when interpreting the RET values, given the small samples analysed for most extinct taxa, which preclude analysing sexes or dental loci separately, and the confounding effects of both sexual dimorphism (lower 2D RET values in males) and tooth position (2D RET increases from first to third molars; Smith et al. 2005, 2012b, 2019). This is highlighted by the 2D RET results newly reported here for *H. crusafonti* and especially *H. laietanus*, since the comparatively larger sample for the latter species shows a wide range of variation (10.3–19.1 μm; Table 2, see Fortuny et al. 2021, SI fig. 6) that almost encompasses all the remaining taxa. Similarly, all the extant taxa represented by adequate samples display a wide range of variation in 2D and 3D RET (with maximum values often almost doubling minimum values). Sexual dimorphism might play some role in this regard, given that Smith et al. (2012b) found higher 2D RET values for male than for female orangutans, although differences were not significant for molar loci except in the M3, and differences between tooth loci appear to be larger. All of these factors cannot be adequately addressed with the studied sample, and caution is warranted for extinct taxa represented by small samples. Among

hominoids from Catalonia, only *H. laietanus* (N = 17) is well represented, although the samples of *P. catalaunicus* (N = 5), *A. brevirostris* (N = 9) and *H. crusafonti* (N = 7) are still greater than for most other extinct apes except for *Griphopithecus* (N = 8), *Rudapithecus hungaricus* (N = 8) and *Gigantopithecus blacki* (N = 7). While 3D RET is useful for comparing the Iberian dryopithecines with one another and with extant hominoids, comparisons with most extinct hominoids are generally limited to 2D RET data (Smith et al. 2019). This is problematic because, even though 2D and 3D RET results are more informative because they reflect the global pattern of enamel distribution. Taken together, the data reported here both in 2D and 3D support the view that Iberian dryopithecines, like *Rudapithecus* from Hungary and Danuvius from Germany (see below), are thicker-enamelled than African apes (especially gorillas), and most similar to the condition displayed by extant gibbons and, to a lesser extent, orangutans. However, there are exceptions: *'S.' occidentalis* (which clearly displays thicker enamel, most similar to *Griphopithecus*) and *P. catalaunicus* (which more closely approaches the orangutan condition, particularly in 3D). The 2D RET for *Rudapithecus* (14.35 μm, range 11.29–17.48 μm, N = 8; Smith et al. 2019) fits well with the ranges reported for most Iberian dryopithecines except *'S.' occidentalis* (and particularly with the variation displayed by *H. laietanus*), whereas Danuvius (16.03 μm, N = 1; Bohme et al. 2019) is most similar to *P. catalaunicus* based on the single reported figure for this taxon (a second molar). There is the possibility that *D. fontani* and *H. crusafonti* display thinner enamel than the remaining taxa (including *A. brevirostris* and *H. laietanus*), apparently being more similar to chimpanzees, but this cannot be demonstrated based on the small available samples available for these taxa. Assuming that *'S.' occidentalis* belongs to one of the taxa recorded at ACM other than *D. fontani* (Alba et al. 2020), our RET results tentatively support its synonymy with *P. catalaunicus*. As already explained, the RET figures for *'S.' occidentalis* are probably exaggerated because there is no first molar available; combining this sample with that of *P. catalaunicus* would result in a taxon with an enamel thickness most similar to orangutans. In contrast, combining the *'S.' occidentalis* sample with that of *A. brevirostris* would result in an even wider range of variation than that documented for *H. laietanus*. Hominoids as a whole are generally thicker-enamelled than other anthropoids (Olejniczak et al. 2008a), although displaying considerable interspecific variation (Martin 1985; Schwartz 2000; Smith et al. 2005, 2008; Olejniczak et al. 2008a). Enamel thickness is labile in evolutionary terms due to convergent and relatively rapid dietary adaptations (Andrews & Martin 1991; Alba et al. 2010b). Thick enamel, in particular, has been classically linked to sclerocarpy (the consumption of hard-food items; Martin 1985; Andrews & Martin 1991; Vogel et al. 2008). This has been related to selection pressures for low cusp relief and reduced shearing crests (Andrews & Martin 1991) or the biomechanical need to prevent the propagation of radial cracks from the EDJ during the mastication of hard foods (Vogel et al. 2008). However, although there seems to be some general correspondence between the overall properties of the food habitually consumed and tooth structure in primates, linking enamel thickness with specific diets is not always possible, especially in instances where phylogenetically closely-related species that consume different kinds of food are considered (Grine & Daegling 2017). Our 2D RET results suggest that most of the Iberian Miocene dryopithecines present thicker enamel than African apes (especially gorillas) and in some cases also than siamangs, which display folivorous tendencies despite a mainly frugivorous diet. In contrast, RET results from Iberian fossil dryopithecines are virtually identical to those of gibbons, and apparently somewhat lower than those of orangutans. This agrees with a soft frugivorous diet for Iberian dryopithecines, with the exception of *Pierolapithecus*. The latter more closely resembles orangutans, which, unlike gibbons, include a scleroparpic component in their diet. This is consistent with microwear data suggesting a

frugivorous diet with an orang-like, arboreal hard-object component for *Pierolapithecus* (DeMiguel et al. 2014), but lacking a specialized hard-object diet such as that inferred for *Griphopithecus*. The hypothesis that thick enamel and other dentognathic adaptations to sclerocarpic feeding were the key adaptation that facilitated the dispersal of hominoids out of Africa into Eurasia (Begun 2003) was favoured based on previous data (Alba et al. 2010b) indicating that both *Pierolapithecus* and *Anoiapithecus* were as thick-enamelled as earlier African afropithecids (Afropithecus), Eurasian putative stem hominids (*Griphopithecus*), and early pongines from Asia (Sivapithecus). Our results do not disprove this view, based on the earliest Eurasian forms (*Griphopithecus*), but indicate that it cannot be supported further based on Iberian dryopithecines, which display an enamel thickness and microwear signal overall more in agreement with soft frugivory (Alba et al. 2010b; DeMiguel et al. 2014). Whether the apparently thicker-enamelled *Pierolapithecus* (particularly if *'S.' occidentalis* belongs to the same taxon) retains the plesiomorphic condition or represents a secondary reversal among the dryopithecine radiation cannot be determined. Enamel distribution maps Enamel distribution maps further enable a more refined assessment of enamel thickness, as it has been shown that molar enamel thickness distribution may differ between taxa with close 3D RET values, indicating that the latter might not adequately reflect molar functional and/or taxonomic signals (Kono 2004; Kono & Suwa 2008; Macchiarelli et al. 2008, 2009; Olejniczak et al. 2008b, c; Suwa & Kono 2005; Suwa et al. 2009). Enamel distribution maps of the upper molars of Miocene dryopithecines from Catalonia show that *P. catalaunicus*, *A. brevirostris*, *D. fontani* and *H. laietanus* exhibit a similar pattern, with the thickest enamel lying over the talon and lateral cusp walls, and the trigon basin being considerably thinner (in *D. fontani*) to moderately thinner (in the other taxa). In this regard, dryopithecines differ from extant apes, with Pan and Hylobates exhibiting their thickest enamel peripherally (on the external aspect of the cusps) and much thinner occlusal enamel, and Gorilla and Pongo approximating this pattern but displaying relatively thicker occlusal enamel (Kono 2004; Kono & Suwa 2008; Suwa et al. 2009). While enamel distribution in the upper molars does not differ among the investigated taxa, for the lower molars it shows differences between *H. laietanus* and *H. crusafonti*. The distinction between these species and the inclusion of the mandible MGSB25314 in *H. crusafonti* instead of *D. fontani* has been supported by some authors (Begun 1992, 2002; Alba 2012; Alba et al. 2012b, 2013) but questioned by others (Harrison 1991; Golpe Posse 1993; Ribot et al. 1996). The only examined lower molar of *H. crusafonti* from its type locality differs from most specimens of *H. laietanus* by displaying the thickest enamel on the buccal aspect of the buccal cusps instead of the periphery of the whole talonid, thereby supporting their distinction. The molars from the mandible MGSB25314 also differ from those of *H. laietanus*. Nevertheless, they differ in a different way than the aforementioned paratype of *H. crusafonti*, by displaying the thickest enamel on the external aspect of all cusps. This is consistent with an assignment of MGSB25314 to a species other than *H. laietanus*, but it does not particularly support its assignment to *H. crusafonti*. The taxonomic conclusions drawn from these comparisons must remain tentative given the small sample of lower molars available for *H. crusafonti* from the type locality, the lack of enamel distribution maps for mandibular specimens of *D. fontani* from its type locality (Saint-Gaudens, France), and the fact that a particular specimen of *H. laietanus* (the invalid holotype of *Dryopithecus* piveteaui nomen nudum) more closely resembles the single examined paratype of *H. crusafonti*. In turn, the enamel distribution of *'S.' occidentalis* specimens, characterized by the presence of thicker areas mostly on the buccal half of the crown and thinner lingual enamel further supports their attribution to a single taxon. However, the restricted sample sizes available (especially the lack of lower molar distribution maps for *P. catalaunicus* and *A. brevirostris*, which are potentially

conspecific with *'S.' occidentalis*; Alba et al. 2020) and further similarities with some specimens of *Hispanopithecus* (notably IPS1822) preclude a conclusive assessment of the taxonomic implications of enamel distribution. EDJ morphology Contrasting with the traditional emphasis on OES for assessing dental morphology, the usefulness of the EDJ has been recently stressed (Olejniczak et al. 2004; Skinner 2008; Skinner et al. 2008a, 2009b, Skinner et al. 2008b, 2009a; Zanolli et al. 2012, 2014; Zanolli & Mazurier 2013; Davies et al. 2019; Detroit et al. 2019) given that it provides highly-diagnostic additional information for taxonomic identification (Smith et al. 2006; Skinner et al. 2008a, b, 2009a, b; Zanolli et al. 2012, 2014, 2016, 2019); and enables tooth morphology comparisons irrespective of occlusal wear (Tables 3 and 4). The thicker and more inflated crests, secondary enamel folds, and cusp bases that distinguish *P. catalaunicus* from A. brevisrostris and *D. fontani* at the OES (Alba et al. 2013; Perez de los Rıos et al. 2013) are not reflected at the EDJ, and are thus probably attributable to the overall thicker enamel of the former. However, *P. catalaunicus* also differs from these genera in other upper molar features observable at the EDJ: from *D. fontani*, in the deeper trigon basin, the higher and straighter crista obliqua, the M1 hypocone dentine horn more aligned with that of the protocone (in agreement with OES morphology; Alba et al. 2013; Perez de los Rıos et al. 2013), the less buccolingually waisted upper molars, and the less developed lingual cingulum; and from *A. brevirostris*, in the shallower and less restricted mesial fovea, the M1 and M2 hypocone horn less lingually situated relative to that of the protocone (in agreement with the OES morphology; Alba et al. 2013; Perez de los Rıos et al. 2013), the markedly less buccolingually waisted upper molars, and the much less developed lingual cingulum. As previously reported (Alba et al. 2020), the EDJ morphology of the ACM/BCV4 specimen supports its conspecificity with the holotype of *'S.' occidentalis*, only differing in the lack of a tuberculum intermedium in the former, which is variable in *H. crusafonti* and hence likely to be attributable to intraspecific variation. These similarities (and those in enamel thickness and distribution mentioned above) strengthen the attribution of the ACM/BCV4 specimen to the same taxon as the holotype of *'S.' occidentalis* (Alba et al. 2020). The latter specimen (originally consisting of a mandibular fragment, but currently preserved as isolated M2 and M3; Golpe Posse 1993) was initially assigned to *D. fontani* (Villalta Comella & Crusafont Pairo 1941) but soon thereafter used to erect a new species (de Villalta Comella & Crusafont Pairo 1944). Over the years, *'S.' occidentalis* has been mostly synonymized with *Hispanopithecus* laietanus (or *Dryopithecus* laietanus) (Crusafont-Pairo & Hurzeler 1961; Simons & Pilbeam 1965; Begun et al. 1990; Harrison 1991; Golpe Posse 1993; Ribot et al. 1996), later considered to be nomen dubium (Moyà-Solà et al. 2004, 2009a; Casanovas-Vilar et al. 2011; Alba 2012; Marigo et al. 2014; Alba et al. 2017) and recently considered to be species inquirenda (Alba et al. 2020). In particular, based on 2D RET and both EDJ and OES similarities, it was recently concluded that *'S.' occidentalis* is not synonymous with *D. fontani*, but given the lack of well-preserved M2 of *A. brevirostris* it was not possible to favour a synonymy with *P. catalaunicus* over the latter species (Alba et al. 2020). The 3D RET results reported above tentatively support the view that *'S.' occidentalis* represents the otherwise unknown lower dentition of *P. catalaunicus*, in which case the former species epithet would take priority. On the other hand, we consider it inadvisable to formally synonymize these taxa until an alternative assignment to *A. brevirostris* can be more convincingly excluded based on additional mandibular material unequivocally assignable to *P. catalaunicus* (i.e. ideally associated with cranial remains). The EDJ morphology is also informative regarding the alpha-taxonomy of *Hispanopithecus*, which was erected with *H. laietanus* as its type species by Villalta Comella & Crusafont Pairo (1944) but later synonymized with *Dryopithecus* (Simons & Pilbeam 1965). For many years, such synonymy was accepted by most authors (Begun et al. 1990; Harrison 1991;

Begun 1992, 2002, 2007; Moyà-Solà & Kohler 1993, 1995; Ribot et al. 1996; Andrews et al. 1996), with only a few exceptions (Golpe Posse 1993; Cameron 1997, 1998, 1999). Indeed, *H. crusafonti* was originally described within *Dryopithecus* (Begun 1992) and subsequently reallocated to *Hispanopithecus* by only a few authors (e.g. Cameron 1999) until the discovery of ACM dryopithecines permitted the reestablishment of the distinct generic status of *Hispanopithecus* on a firmer basis (Moyà-Solà et al. 2009a; Begun 2009). This has subsequently been accepted by most authors (Begun 2010, 2015; Moyà-Solà et al. 2009b; Casanovas-Vilar et al. 2011; Alba 2012; Alba et al. 2012b, 2013; Alba & Moyà-Solà 2012; Begun et al. 2012; Perez de los Rıos et al. 2013; Fleagle 2013; Bohme et al. 2019) with only a few exceptions (Pickford 2012) regarding *H. crusafonti*. Our results show that the late Miocene *H. laietanus* and *H. crusafonti* differ from the investigated middle Miocene taxa in the more peripheral dentine horns of the upper molars (especially in *H. laietanus*) as well as in the lower and often disrupted crista obliqua. They further differ from *P. catalaunicus* and *D. fontani*, but not *A. brevirostris*, in the deeper and more restricted mesial fovea, and the somewhat more marked buccolingual waisting of the upper molars (although this feature is variable). All these features support the distinction of the genus *Hispanopithecus* from *Dryopithecus* and other middle Miocene dryopithecine genera from the Valles-Penedes Basin. It is noteworthy that the distinction of *H. crusafonti* from *H. laietanus* (Begun 1992, 2002, 2009; Cameron 1999; Moyà-Solà et al. 2009a; Casanovas-Vilar et al. 2011; Alba 2012; Alba & Moyà-Solà 2012; Alba et al. 2012b; Pickford 2012) was questioned (Andrews et al. 1996) or even disputed (Harrison 1991; Ribot et al. 1996) by some authors, who considered the former to be a junior subjective synonym of the latter. The original diagnosis of *H. crusafonti* (Begun 1992) mentioned a series of differences in tooth size and shape relative to *H. laietanus* that were later re-evaluated based on an enlarged sample of upper teeth attributed to the latter species (Alba et al. 2012b). Such re-evaluation concluded that incisor morphology and cheek teeth proportions tentatively supported the distinction of two species, while the development of cingula was too variable to serve as a taxonomically valid criterion. In fact, the original claim that *H. crusafonti* displays more reduced cingula than *H. laietanus* (Begun 1992; Cameron 1999) had already been rejected based on the OES morphology (Ribot et al. 1996; Alba et al. 2013). In turn, the presence of a more median hypocone and a better developed metacone in the M3 of *H. crusafonti* was considered to be potentially diagnostic, although with doubts due to the small samples available and the high variability displayed by the M3 of *H. laietanus* (Alba et al. 2012b). Our assessment of the EDJ morphology suggests that the two latter features are too variable to be diagnostic, but leads us to identify alternative additional diagnostic features in the upper molars, namely the more lingual position of the M1 and M2 hypocone, the less peripheral dentine horns, the deeper trigon basin, and the more developed lingual cinglum in *H. crusafonti*. It is particularly noteworthy that, at the EDJ, *H. crusafonti* displays better developed cingula than *H. laietanus*, contrary to the conclusions in the original description of the former species (Begun 1992), which relied on OES morphology. Concerning the lower molars, several distinctive features noted in the original description (deep and narrow grooves between the buccal cuspids or shallower and more restricted talonid basins; Begun 1992) are not reflected in EDJ morphology. In contrast, *H. crusafonti* (including the specimen MGSB25314) displays a more developed buccal cingulid at the EDJ and less pronounced buccolingual waisting of the lower molars than *H. laietanus*. Therefore, the EDJ evidence provided here for both upper and lower molars, coupled with cheek tooth proportions and upper incisor morphology (Alba et al. 2012b), support the distinction of the two *Hispanopithecus* species. It should also be mentioned that, as previously noted for the OES (Alba et al. 2013), for some features (moderately peripheral upper molar dentine horns) *H. crusafonti* more closely resembles the middle Miocene hominoids

(especially *A. brevirostris*: deeper trigon basin, lingually-positioned hypocone dentine horn, more developed lingual cingulum) than *H. laietanus* does. These features appear to be plesiomorphic and might indicate a more basal position for *H. crusafonti*, although additional (especially cranial) remains would be required to further test this hypothesis. Finally, although a single dryopithecine species is customarily recognized at Can Llobateres (Begun et al. 1990; Harrison 1991; Begun 1992, 2002; Moyà-Solà & Kohler 1993, 1995; Andrews et al. 1996; Ribot et al. 1996; Cameron 1997, 1999; Casanovas-Vilar et al. 2011; Alba & Moyà-Solà 2012; Alba et al. 2012b), this is worth revising in the light of the EDJ data reported here, particularly given previous proposals that two additional species might be represented at this site (Crusafont-Pairo & Hurzeler 1961, 1969; Crusafont-Pairo & Golpe-Posse 1973): a smaller species ('Rahonapithecus sabadellensis') and a larger one ('*Dryopithecus* piveteaui'). Although these species are nomenclaturally invalid (nomina nuda) (Simons & Pilbeam 1965; Begun et al. 1990; Alba & Moyà-Solà 2012; Alba et al. 2012b), some authors have considered that the purported holotype of 'Rahonapithecus sabadellensis' (IPS1802, a mandibular fragment with M1–M3) might belong to the same taxon as the holotype of *'S.' occidentalis* (Pickford 2012). Even if the M3 of this specimen displays the thickest value among the sample of this locality, this is not the case for 3D RET, and overall the wide range of 2D RET values displayed by *H. laietanus* conform to the levels of variation displayed by extant great ape species (see Fortuny et al. 2021, table 7, SI fig. 6). The lower molars from Can Llobateres 1, despite some variation in EDJ morphology (e.g. in the presence of M2 metaconulid), do not show marked differences that might justify the distinction of additional species, and are characterized by the same features (e.g. poorly developed buccal cingulid and marked buccolingual waisting) that distinguish the holotype of *H. laietanus* from the remaining investigated taxa. The same applies to the EDJ morphology of the purported holotype of 'D. piveteaui' (IPS1822, an M3 germ). This specimen merely stands out by its marked development of enamel wrinkling at the OES, which is not reflected in any concomitant differences from other *H. laietanus* specimens at the EDJ and is likely to be attributable to a lack of wear.

Conclusion

Our reassessment of Iberian dryopithecine palaeobiodiversity in the light of the reported data on tooth endostructural morphology is consistent with the distinction of four different genera and five species of Miocene dryopithecines in Catalonia; these taxa were originally based on cranial morphology and features of the outer enamel surface. Our conclusions therefore reinforce the view that neither *Pierolapithecus*, *Anoiapithecus* nor *Hispanopithecus* can be considered junior synonyms of *Dryopithecus*. This also holds for *'S.' occidentalis*, which must remain a species inquirenda until additional lower molars of *P. catalaunicus* or *A. brevirostris* enable further comparisons. Our results also show that the two late Miocene species of dryopithecines from Catalonia (included in *Hispanopithecus*) display several derived features as compared to the middle Miocene taxa. However, *H. crusafonti* generally retains a more primitive morphology than *H. laietanus* and is thus more similar to the middle Miocene genera. In the future, other aspects of the internal structure of the post-canine teeth of these Miocene hominids and other extinct apes from Europe will be investigated to extract additional palaeobiological information. In particular, analyses of root morphology (e.g. Kupczik & Hublin 2010; Kupczik et al. 2019; Moore et al. 2013, 2016; Pan et al. 2019) and the application of morphometric geometric techniques to quantify the EDJ shape (e.g. Skinner et al. 2009b, 2016; Zanolli et al. 2018, 2019) will further highlight Miocene hominid diversity. However, pending the recovery and analysis of additional craniodental remains from Europe (such as those of Danuvius; Bohme et al. 2019) this

study confirms the need for 3D tooth endostructural analyses in studies aimed at assessing the alpha-taxonomy of fossil apes, as noted by some previous studies (Zanolli et al. 2019). The application of these techniques to currently available isolated dentognathic fragments from elsewhere in Europe might ultimately unveil further the previously unrecognized palaeobiodiversity of Miocene apes in this continent.

Acknowledgements
This work was funded by the Spanish Agencia Estatal de Investigacion–European Regional Development Fund of the European Union (CGL2016-76431-P and CGL2017- 82654-P, AEI/FEDER-UE), the Generalitat de Catalunya (CERCA Program and consolidated research groups 2017 SGR 086 and 2017 SGR 116), the French CNRS, and the Regione Friuli- Venezia Giulia (ICTP/Elettra EXACT Project) in the frame of the SAPIENS Project funded by the Centro Fermi. We thank Sergio Llacer for image processing, and Sebastia Calzada for the loan of specimens housed at the MGSB. We thank Jay Kelley for constructive input on an early version of this manuscript, as well as two anonymous reviewers for their helpful comments on the original version submitted to the journal.

Data Archiving Statement
Digital surface models of the OES and EDJ of the investigated molars are available on MorphoSource (https://www.morphosource. org/projects/0000C1160). OES models are openly shared; the EDJ are available on request; see the Dryad Digital Repository (https://doi. org/10.5061/dryad.573n5tb5t) for a list of DOIs and additional data and supplementary information. MicroCT raw data requests should be addressed to the Fieldwork & Collection Management Area of the ICP (https://www.icp.cat/index. php/en/icp-2/equip).

References
ALBA, D.M. 2012. Fossil apes from the Vallès-Penedès Basin. *Evolutionary Anthropology*, **21**, 254–269.
— and MOYÀ-SOLÀ, S. 2012. On the identity of a hominoid male upper canine from the Vallès-Penedès Basin figured by Pickford. *Estudios Geológicos*, **68**, 149–153.
— — CASANOVAS-VILAR, I., GALINDO, J., ROBLES, J.M., ROTGERS, C., FURIÓ, M., ANGELONE, C., KÖHLER, M., GARCÉS, M., CABRERA, L., ALMÉCIJA, S. and OBRADÓ, P. 2006. Los vertebrados fósiles del Abocador de Can Mata (els Hostalets de Pierola, l'Anoia, Cataluña), una sucesión de localidades del Aragoniense superior (MN6 y MN7+8) de la cuenca del Vallès-Penedès. Campañas 2002–2003, 2004 y 2005. *Estudios Geológicos*, **62**, 295–312.
— — MALGOSA, A., CASANOVAS-VILAR, I., ROBLES, J.M., ALMÉCIJA, S., GALINDO, J., ROTGERS, C. and BERTÓ MENGUAL, J.V. 2010*a*. A new species of *Pliopithecus* Gervais, 1849 (Primates: Pliopithecidae) from the Middle Miocene (MN8) of Abocador de Can Mata (els Hostalets de Pierola, Catalonia, Spain). *American Journal of Physical Anthropology*, **141**, 52–75.
— FORTUNY, J. and MOYÀ-SOLÀ, S. 2010*b*. Enamel thickness in the Middle Miocene great apes *Anoiapithecus, Pierolapithecus* and *Dryopithecus*. *Proceedings of the Royal Society B*, **277**, 2237–2245.
— ALMÉCIJA, S., and MOYÀ-SOLÀ, S. 2010*c*. Locomotor inferences in *Pierolapithecus* and *Hispanopithecus*: Reply to Deane and Begun (2008). *Journal of Human Evolution*, **59**, 143–149.

— MOYÀ-SOLÀ, S., and ALMÉCIJA, S. 2011. A partial hominoid humerus from the middle Miocene of Castell de Barberà (Vallès-Penedès Basin, Catalonia, Spain). *American Journal of Physical Anthropology*, **144**, 365–381.
— — ROBLES, J.M., and GALINDO, J. 2012*a*. The oldest pliopithecid record in the Iberian Peninsula based on new material from the Vallès-Penedès Basin. *American Journal of Physical Anthropology*, **147**, 135–140.
— CASANOVAS-VILAR, I., ALMÉCIJA, S., ROBLES, J.M., ARIAS-MARTORELL, J. and MOYÀ-SOLÀ, S. 2012*b*. New dental remains of *Hispanopithecus laietanus* (Primates: Hominidae) from Can Llobateres 1 and the taxonomy of Late Miocene hominoids from the Vallès-Penedès Basin (NE Iberian Peninsula). *Journal of Human Evolution*, **63**, 231–246.
— ALMÉCIJA, S., CASANOVAS-VILAR, I., MÉNDEZ, J.M., MOYÀ-SOLÀ, S. 2012*c*. A partial skeleton of *Hispanopithecus laietanus* from Can Feu and the mosaic evolution of crown-hominoid positional behaviors. *PLoS ONE*, **7**, e39617.
— FORTUNY, J., PÉREZ DE LOS RÍOS, M., ZANOLLI, C., ALMÉCIJA, S., CASANOVAS-VILAR, I., ROBLES, J.M. and MOYÀ-SOLÀ, S. 2013. New dental remains of *Anoiapithecus* and the first appearance datum of hominoids in the Iberian Peninsula. *Journal of Human Evolution*, **65**, 573–584.
— ALMÉCIJA, S., DEMIGUEL, D., FORTUNY, J., PÉREZ DE LOS RÍOS, M., PINA, M., ROBLES, J.M. and MOYÀ-SOLÀ, S. 2015. Miocene small-bodied ape from Eurasia sheds light on hominoid evolution. *Science*, **350**, aab2625.
— CASANOVAS-VILAR, I., GARCÉS, M. and ROBLES, J.M. 2017. Ten years in the dump: An updated review of the Miocene primate-bearing localities from Abocador de Can Mata (NE Iberian Peninsula). *Journal of Human Evolution*, **102**, 12–20.
— FORTUNY, J., ROBLES, J.M., BERNARDINI, F., PÉREZ DE LOS RÍOS, M., TUNIZ, C., MOYÀ-SOLÀ, S. and ZANOLLI, C. 2020. A new dryopithecine mandibular fragment from the middle Miocene of Abocador de Can Mata and the taxonomic status of '*Sivapithecus' occidentalis* from Can Vila (Vallès-Penedès Basin, NE Iberian Peninsula. *Journal of Human Evolution*, **145**, 102790.
ALMÉCIJA, S., ALBA, D. M., MOYÀ-SOLÀ, S., and KÖHLER, M. 2007. Orang-like manual adaptations in the fossil hominoid *Hispanopithecus laietanus*: first steps towards great ape suspensory behaviours. *Proceedings of the Royal Society B*, **274**, 2375–2384.
— — — 2009. *Pierolapithecus* and the functional morphology of Miocene ape hand phalanges: paleobiological and evolutionary implications. *Journal of Human Evolution*, **57**, 284–297.
— TALLMAN, M., ALBA, D.M., PINA, M., MOYÀ-SOLÀ, S., and JUNGERS, W.L. 2013. The femur of *Orrorin tugenensis* exhibits morphometric affinities with both Miocene apes and later hominins. *Nature Communications*, **4**, 2888.
ANDREWS, P., 2020. Last common ancestor of apes and humans: Morphology and environment. *Folia Primatologica*, **91**, 122–148.
— and MARTIN, L. 1991. Hominoid dietary evolution. *Philosophical Transactions of the Royal Society B*, **334**, 199–209.
— HARRISON, T., DELSON, E., BERNOR, R. L. and MARTIN, L. 1996. Distribution and biochronology of European and Southwest Asian Miocene catarrhines. 168–207. *In* BERNOR, R.L., FAHLBUSCH, V. and MITTMANN, H.-W (eds). *The Evolution of Western Eurasian Neogene Mammal Faunas*. Columbia University Press, Columbia, 528 pp.

BAYLE, P., BONDIOLI, L., MACCHIARELLI, R., MAZURIER, A., PUYMERAIL, L., VOLPATO, V. and ZANOLLI, C. 2011. Three-dimensional imaging and quantitative characterization of human fossil remains. Examples from the Nespos database. 29–46. *In* MACCHIARELLI, R. and WENIGER G.-C. (eds). *Pleistocene Databases. Acquisition, Storing, Sharing.* Wissenschaftliche Schriften des Neanderthal Museums, Mettmann **4**, 121 pp.

BEGUN, D.R. 1992. *Dryopithecus crusafonti* sp. nov., a new Miocene hominoid species from Can Ponsic (Northeastern Spain). *American Journal of Physical Anthropology*, **87**, 291–309.

— 2002. European hominoids. 339–368. *In* HARTWIG, W.C. (ed). *The Primate Fossil Record*. Cambridge University Press, Cambridge, 503 pp.

— 2003. Planet of the apes. *Scientific American*, **289**, 74–83.

— 2007. Fossil record of Miocene hominoids. 921–977. *In* HENKE, W. and TATTERSALL, I. (eds). *Handbook of Paleoanthropology*. Springer Verlag, Berlin, 2069 pp.

— 2009. Dryopithecins, Darwin, de Bonis, and the European origin of the African apes and human clade. *Geodiversitas*, **31**, 789–816.

— 2010. Miocene hominids and the origins of the African apes and humans. *Annual Review of Anthropology*, **39**, 67–84.

— 2015. Fossil record of Miocene hominoids. 1261–1332. *In* HENKE, W. and TATTERSALL, I. (eds). *Handbook of Paleoanthropology.* Springer Verlag, Berlin, 2624 pp.

— MOYA-SOLA, S. and KOHLER, M. 1990. New Miocene hominoid specimens from Can Llobateres (Vallès Penedès, Spain) and their geological and paleoecological context. *Journal of Human Evolution*, **19**, 255–268.

— NARGOLWALLA, M. C. and KORDOS, L. 2012. European Miocene hominids and the origin of the African ape and human clade. *Evolutionary Anthropology*, **21**, 10–23.

BENAZZI, S., PANETTA, D., FORNAI, C., TOUSSAINT, M., GRUPPIONI, G. and HUBLIN, J.J. 2014. Guidelines for the digital computation of 2D and 3D enamel thickness in hominoid teeth. *American Journal of Physical Anthropology*, **153**, 305–313.

BÖHME, M., SPASSOV, N., FUSS, J., TRÖSCHER, A., DEANE, A.S., PRIETO, J., KIRSCHER, U., LECHNER, T. and BEGUN, D.R., 2019. A new Miocene ape and locomotion in the ancestor of great apes and humans. *Nature*, **575**, 489–493.

CAMERON, D.W. 1997. A revised systematic scheme for the Eurasian Miocene fossil Hominidae. *Journal of Human Evolution*, **33**, 449–477.

— 1998. Patterns of faciodental sexual dimorphism in *Hispanopithecus*. *Zeitschrift für Morphologie und Anthropologie*, **82**, 47–58.

— 1999. The single species hypothesis and *Hispanopithecus* fossils from the Vallés Penedés Basin, Spain. *Zeitschrift für Morphologie und Anthropologie*, **82**, 159–186.

CASANOVAS-VILAR, I., ALBA, D.M., GARCÉS, M., ROBLES, J.M. and MOYÀ-SOLÀ, S. 2011. Updated chronology for the Miocene hominoid radiation in Western Eurasia. *Proceedings of the National Academy of Sciences of the United States of America*, **108**, 5554–5559.

— GARCÉS, M., VAN DAM, J.A., GARCÍA PAREDES, I., ROBLES, J.M. and ALBA, D.M. 2016. An updated biostratigraphy for the late Aragonian and Vallesian of the Vallès-Penedès Basin (Catalonia). *Geologica Acta*, **14**, 195–217.

COLEMAN, M.N. and COLBERT, M.W. 2007. CT thresholding protocols for taking measurements on three-dimensional models. *American Journal of Physical Anthropology*, **133**, 723–725.

CRUSAFONT-PAIRO, M. and HÜRZELER, J., 1961. Les Pongidés fossiles d'Espagne. *Comptes Rendus de l'Académie des Science*, Paris **252**, 582–584.

— — 1969. Catálogo comentado de los póngidos fósiles de España. *Acta Geologica Hispánica*, **4**, 44–48.

— and GOLPE-POSSE, J.M. 1973. New pongids from the Miocene of Vallès Penedès Basin (Catalonia, Spain). *Journal of Human Evolution*, **2**, 17–24.

DAVIES, T.W., DELEZENE, L. K., GUNZ, P., HUBLIN, J.-J. and SKINNER, M. M. 2019. Endostructural morphology in hominoid mandibular third premolars: Discrete traits at the enamel-dentine junction. *Journal of Human Evolution*, **136**, 102670.

DEMIGUEL, D., ALBA, D.M. and MOYÀ-SOLÀ, S. 2014. Dietary specialization during the evolution of Western Eurasian hominoids and the extinction of European great apes. *PLoS One*, **9**, e97442.

DETROIT, F., MIJARES, A.S., CORNY, J., DAVER, G., ZANOLLI, C., DIZON, E., ROBLES, E., GRÜN, R. and PIPER, P.J. 2019. A new species of *Homo* from the Late Pleistocene of the Philippines. *Nature*, **568**, 181–186.

FAJARDO, R.J., RYAN, T.M. and KAPPELMAN J. 2002. Assessing the accuracy of high resolution X-ray computed tomography of primate trabecular bone by comparisons with histological sections. *American Journal of Physical Anthropology*, **118**, 1–10.

FLEAGLE, J.G. 2013. *Primate Adaptation and Evolution*, 3rd ed. Academic Press, London, 464 pp.

FORTUNY, J., ZANOLLI, C., BERNARDINI, F., TUNIZ, C. and ALBA, D.M. 2020. Data from: Dryopithecine palaeobiodiversity in the Iberian Miocene revisited on the basis of molar endostructural morphology.

GOLPE-POSSE, J.M. 1993. Los Hispanopitecos (Primates, Pongidae) de los yacimientos del Vallès-Penedès (Cataluña, España). II: Descripción del material existente en el Instituto de Paleontología de Sabadell. *Paleontologia i Evolució*, **26–27**, 151–224.

GRINE, F.E. 2002. Scaling of tooth enamel thickness, and molar crown size reduction in modern humans. *South African Journal of Science*, **98**, 503–509.

— 2005. Enamel thickness of deciduous and permanent molars in modern *Homo sapiens*. *American Journal of Physical Anthropology*, **126**, 14–31.

GRINE, F.E. and DAEGLING, D.J. 2017. Functional morphology, biomechanics and the retrodiction of early hominin diets. *Comptes Rendus Palevol*, **16**, 613–631.

— and MARTIN, L.B. 1988. Enamel thickness and development in *Australopithecus* and *Paranthropus*. 3–42. *In* GRINE, F.E (ed). *Evolutionary History of the "Robust" Australopithecines*. Aldine de Gruyter, Berlin, 550 pp.

HAMMER, Ø., HARPER, D.A.T. and RYAN, P.D. 2001. PAST: Paleontological statistics software package for education and data analysis. *Palaeontologia Electronica*, **4**, 4.

HARRISON, T. 1991. Some observations on the Miocene hominoids from Spain. *Journal of Human Evolution*, **19**, 515–520.

— and GU, Y. 1999. Taxonomy and phylogenetic relationships of early Miocene catarrhines from Sihong, China. *Journal of Human Evolution*, **37**, 225–277.

KELLEY, J. DEAN, M.C. and REID, D.J. 2001. Molar growth in the late Miocene hominoid, *Dryopithecus laietanus*. 123–134. *In* BROOK, A. (ed). *Dental Morphology 2001: 12th International Symposium on Dental Morphology*. Sheffield Academic Press, Sheffield, 350 pp.

KONO, R. 2004. Molar enamel thickness and distribution patterns in extant great apes and humans: New insights based on a 3-dimensional whole crown perspective. *Anthropological Science*, **112**, 121–146.
— and SUWA, G. 2008. Enamel distribution patterns of extant human and hominoid molars: Occlusal versus lateral enamel thickness. *Bulletin of the National Museum of Nature and Science, Series D*, **34**, 1–9.
MACCHIARELLI, R., BONDIOLI, L. and MAZURIER, A. 2008. Virtual dentitions: touching the hidden evidence. 426–448. *In* IRISH, J.D., NELSON, G.C. (eds), *Technique and Application in Dental Anthropology*. Cambridge University Press, Cambridge, 470 pp.
— MAZURIER, M., ILLERHAUS, B. and ZANOLLI, C. 2009. *Ouranopithecus macedoniensis*: virtual reconstruction and 3D analysis of a juvenile mandibular dentition (RPl-82 and RPl-83). *Geodiversitas*, **31**, 851–863.
— BAYLE, P., BONDIOLI, L., MAZURIER, A., ZANOLLI, C. 2013. From outer to inner structural morphology in dental anthropology: integration of the third dimension in the visualization and quantitative analysis of fossil remains. 250–277. *In* SCOTT, G.R. and IRISH, J.D. (eds), *Anthropological Perspectives on Tooth Morphology. Genetics, Evolution, Variation*. Cambridge University Press, Cambridge, 582 pp.
MACHO, G.A. 1994. Variation in enamel thickness and cusp area within human maxillary molars and its bearing on scaling techniques used for studies of enamel thickness between species. *Archives of Oral Biology*, **39**, 783–792.
MARIGÓ, J., SUSANNA, I., MINWER-BARAKAT, R., MADURELL-MALAPEIRA, J., MOYÀ-SOLÀ, S., CASANOVAS-VILAR, I., ROBLES, J.M. and ALBA, D.M. 2014. The primate fossil record in the Iberian Peninsula. *Journal of Iberian Geology*, **40**, 179–211.
MARTIN, L.B. 1985. Significance of enamel thickness in hominoid evolution. *Nature* **314**, 260–263.
MARTIN-FRANCE S, L., MARTINON-TORRES, M., MARTINEZ DE PINILLOS, M., GARCIA-CAMPOS, C., MODESTO-MATA, M., ZANOLLI , C., RODRIGUEZ, L. and BERMUDEZ DE CASTRO, J. M. 2018. Tooth crown tissue proportions and enamel thickness in Early Pleistocene *Homo antecessor* molars (Atapuerca, Spain). PLoS One, 13, e0203334.
MOYÀ-SOLÀ, S. and KÖHLER, M. 1993. Recent discoveries of *Dryopithecus* shed new light on evolution of great apes. *Nature*, **365**, 543–545.
— — 1995. New partial cranium of *Dryopithecus* Lartet, 1863 (Hominoidea, Primates) from the upper Miocene of Can Llobateres, Barcelona, Spain. *Journal of Human Evolution*, **29**, 101–139.
— — ALBA, D.M., CASANOVAS-VILAR, I. and GALINDO, J. 2004. *Pierolapithecus catalaunicus*, a new Middle Miocene great ape from Spain. *Science*, **306**, 1339–1344.
— — ALBA, D.M., CASANOVAS-VILAR, I. and GALINDO, J. 2005. Response to comment on "*Pierolapithecus catalaunicus*, a new Middle Miocene great ape from Spain". *Science*, **308**, 203d.
— ALBA, D.M., ALMÉCIJA, S., CASANOVAS-VILAR, I., KÖHLER, M., DE ESTEBAN-TRIVIGNO, S., ROBLES, J.M., GALINDO, J. and FORTUNY, J. 2009*a*. A unique Middle Miocene European hominoid and the origins of the great ape and human clade. *Proceedings of the National Academy of Sciences of the United States of America*, **106**, 9601–9606.

— KÖHLER, M., ALBA, D.M., CASANOVAS-VILAR, I., GALINDO, J., ROBLES, J.M., CABRERA, L., GARCÉS, M., ALMÉCIJA, S. and BEAMUD, E. 2009*b*. First partial face and upper dentition of the Middle Miocene hominoid *Dryopithecus fontani* from Abocador de Can Mata (Vallès-Penedès Basin, Catalonia, NE Spain): taxonomic and phylogenetic implications. *American Journal of Physical Anthropology*, **139**, 126–145.
OLEJNICZAK, A.J. 2006. Micro-computed tomography of primate molars. Unpublished PhD thesis, Stony Brook University, New York, 242 pp.
— MARTIN, L.B. and ULHAAS, L. 2004. Quantification of dentine shape in anthropoid primates. *Annals of Anatomy*, **186**, 479–486.
— TAFFOREAU, P., FEENEY, R.N.M. and MARTIN, L.B. 2008*a*. Three-dimensional primate molar enamel thickness. *Journal of Human Evolution*, **54**, 187–195.
— — — — 2008*b*. Three-dimensional molar enamel distribution and thickness in *Australopithecus* and *Paranthropus*. *Biology Letters*, **4**, 406–410.
— SMITH, T.M., WANG, W., POTTS, R., CIOCHON, R., KULLMER, O., SCHRENK, F. AND HUBLIN, J.-J. 2008*c*. Molar enamel thickness and dentine horn height in *Gigantopithecus blacki*. *American Journal of Physical Anthropology*, **135**, 85–91.
— — T.M., FEENEY, R.N., MACCHIARELLI, R., MAZURIER, A., BONDIOLI, L., ROSAS, A., FORTEA, J., DE LA RASILLA, M., GARCIA-TABERNERO, A., RADOVCIC, J., SKINNER, M.M., TOUSSAINT M., and HUBLIN, J.-J. 2008*d*. Dental tissue proportions and enamel thickness in Neandertal and modern human molars. *Journal of Human Evolution*, **55**, 12–23.
PÉREZ DE LOS RÍOS, M., MOYÀ-SOLÀ, S. and ALBA, D.M. 2012. The nasal and paranasal architecture of the Middle Miocene ape *Pierolapithecus catalaunicus* (Primates: Hominidae): Phylogenetic implications. *Journal of Human Evolution*, **63**, 497–506.
— ALBA, D.M. and MOYÀ-SOLÀ, S., 2013. Taxonomic attribution of the La Grive hominoid teeth. *American Journal of Physical Anthropology*, **151**, 558–565.
PICKFORD, M. 2012. Hominoids from Neuhausen and other Bohnerz localities, Swabian Alb, Germany: evidence for a high diversity of apes in the Late Miocene of Germany. *Estudios Geológicos*, **68**, 113–147.
PINA, M., ALBA, D.M., ALMÉCIJA, S., FORTUNY, J., and MOYÀ-SOLA, S. 2012. Brief Communication: Paleobiological inferences on the locomotor repertoire of extinct hominoids based on femoral neck cortical thickness: the fossil great ape *Hispanopithecus laietanus* as a test-case study. *American Journal of Physical Anthropology*, **149**, 142–148.
— — MOYÀ-SOLÀ, S., and ALMÉCIJA, S. 2019. Femoral neck cortical bone distribution of dryopithecin apes and the evolution of hominid locomotion. *Journal of Human Evolution*, **136**, 102651.
RIBOT, F., GIBERT, J. and HARRISON, T. 1996. A reinterpretation of the taxonomy of *Dryopithecus* from Vallès-Penedès, Catalonia (Spain). *Journal of Human Evolution*, **31**, 129–141.
SCHNEIDER, C.A., RASBAND, W.S. and ELICEIRI, K.W. 2012. NIH Image to ImageJ: 25 years of image analysis. *Nature Methods*, **9**, 671–675.
SCHWARTZ, G.T. 2000. Taxonomic and functional aspects of the patterning of enamel thickness distribution in extant large-bodied hominoids. *American Journal of Physical Anthropology*, **111**, 221–244.
SCOTT, G.R and IRISH J.D. 2017. *Human Tooth Crown and Root Morphology. The Arizona State University Dental Anthropology System*. Cambridge University Press, Cambridge, 342 pp.

SIMONS, E. L. and PILBEAM, D. R. 1965. Preliminary revision of the Dryopithecinae (Pongidae, Anthropoidea). *Folia Primatologica*, **3**, 81–152.
SKINNER, M. M. 2008. Enamel-dentine junction morphology of extant hominoid and fossil hominin lower molars. Unpublished Ph.D thesis, The George Washington University, Washington D.C., 191 pp.
— WOOD, B.A., BOESCH, C., OLEJNICZAK, A., ROSAS, A., SMITH, T.M., and HUBLIN, J.-J. 2008*a*. Dental trait expression at the enamel-dentine junction of lower molars in extant and fossil hominoids. *Journal of Human Evolution*, **54**, 173–186.
— GUNZ, P., WOOD, B. A. and HUBLIN, J.-J. 2008*b*. Enamel-dentine junction (EDJ) morphology distinguishes the lower molars of *Australopithecus africanus* and *Paranthropus robustus*. *Journal of Human Evolution*, **55**, 979–988.
— WOOD, B.A. and HUBLIN, J.-J. 2009*a*. Protostylid expression at the enamel-dentine junction and enamel surface of mandibular molars of *Paranthropus robustus* and *Australopithecus africanus*. *Journal of Human Evolution*, **56**, 76–85.
— GUNZ, P., WOOD, B. A., BOESCH, C. and HUBLIN, J.-J. 2009*b*. Discrimination of extant *Pan* species and subspecies using the enamel-dentine junction morphology of lower molars. *American Journal of Physical Anthropology*, **140**, 234–243.
SMITH, H.B. 1984. Patterns of molar wear in hunter-gatherers and agriculturalists. *American Journal of Physical Anthropology*, **63**, 39–56.
SMITH, T.M., OLEJNICZAK, A.J., MARTIN, L.B. and REID, D.J. 2005. Variation in hominoid molar enamel thickness. *Journal of Human Evolution*, **48**, 575–592.
— — REID, D.J., FERRELL, R.J. and HUBLIN J.-J. 2006. Modern human molar enamel thickness and enamel-dentine junction shape. *Archives of Oral Biology*, **51**, 974–995.
— — REH, S., REID, D.J. and HUBLIN, J.-J. 2008. Enamel thickness trends in the dental arcade of humans and chimpanzees. *American Journal of Physical Anthropology*, **136**, 237–241.
— KUPCZIK, K., MACHANDA, Z., SKINNER, M.M. and ZERMENO, J.P. 2012b. Enamel thickness in Bornean and Sumatran orangutan dentitions. *American Journal of Physical Anthropology*, **147**, 417–426.
— TAFFOREAU, P., POUECH, J. and BEGUN, D.R. 2019. Enamel thickness and dental development in *Rudapithecus hungaricus*. *Journal of Human Evolution*, **136**, 102649.
SPOOR, F., ZONNEVELD, F. and MACHO, G.A. 1993. Linear measurements of cortical bone and dental enamel by computed tomography: applications and problems. *American Journal of Physical Anthropology*, **91**, 469–484.
SUWA, G. and KONO, R. T. 2005. A micro-CT based study of linear enamel thickness in the mesial cusp section of human molars: Reevaluation of methodology and assessment of within-tooth, serial, and individual variation. *Anthropological Sciencies*, **113**, 273–289.
SUWA, G., KONO, R.T., SIMPSON, S.W., ASFAW, B., LOVEJOY, C.O. and WHITE, T. 2009. Paleobiological implications of the *Ardipithecus ramidus* dentition. *Science*, **326**, 94–99.
SWINDLER, D.R. 2002. *Primate Dentition. An Introduction to the Teeth of Non-Human Primates*. Cambridge University Press, Cambridge, 296 pp.
THIERY, G., LAZZARI, V., RAMDARSHAN, A. and GUY, F. 2017. Beyond the map: Enamel distribution characterized from 3D dental topography. *Frontiers in Physiology*, **8**, 524.
TURNER, C.G. NICHOL, C.R. and SCOTT, G.R. 1991. Scoring procedures for key morphological traits of the permanent dentition: The Arizona State University Dental Anthropology System. 13–31. *In* KELLEY, L., KELLEY, M. and LARSEN, C.S. (eds), *Advances in Dental Anthropology*. Wiley-Liss, New York, 389 pp.

TUNIZ, C., BERNARDINI, F., CICUTTIN, A., CRESPO, M.-L., DREOSSI, D., GIANONCELLI, A., MANCINI, L., MENDOZA CUEVAS, A., SODINI, N., TROMBA, G., ZANINI, F. and ZANOLLI, C. 2013.The ICTP-Elettra X-ray laboratory for cultural heritage and archaeology. A facility for training and education in the developing world. *Nuclear Instruments and Methods in Physics Research Section A*, **711**, 106–110.

VAN DER MADE, J. and RIBOT, F. 1999. Additional hominoid material from the Miocene of Spain and remarks on hominoid dispersals into Europe. *Contributions to Tertiary and Quaternary Geology*, **36**, 25–39.

VILLALTA COMELLA, J.F. DE and CRUSAFONT PAIRO, M. 1941. Hallazgo del "*Dryopithecus fontani*", Lartet, en el Vindoboniense de la cuenca Vallés-Penedés. *Boletín Instituto Geológico y Minero de España*, **55**, 131–142.

— — 1944. Dos nuevos antropomorfos del Mioceno español y su situación dentro de la moderna sistemática de los símidos. *Notas y Comunicaciones del Instituto Geológico y Minero de España*, **13**, 1–51.

VOGEL, E.R., VAN WOERDEN, J.T., LUCAS, P.W., UTAMI ATMOKO, S.S., VAN SCHAIK, C.P. and DOMINY, N.J. 2008. Functional ecology and evolution of hominoid molar enamel thickness: *Pan troglodytes schweinfurthii* and *Pongo pygmaeus wurmbii*. *Journal of Human Evolution*, **55**, 60–74.

ZANOLLI, C., BONDIOLI, L., MANCINI, L., MAZURIER, A., WIDIANTO, H. and MACCHIARELLI, R. 2012. Two human fossil deciduous molars from the Sangiran Dome (Java, Indonesia): Outer and inner morphology. *American Journal of Physical Anthropology*, **147**, 472–481.

— and MAZURIER, A. 2013. Endostructural characterization of the *H. heidelbergensis* dental remains from the early Middle Pleistocene site of Tighenif, Algeria. *Comptes Rendus Palevol*, **12**, 293–304.

— BONDIOLI, L., COPPA, A., DEAN, C.M., BAYLE, P., CANDILIO, F., CAPUANI, S., DREOSSI, D., FIORE, I., FRAYER, D.W., LIBSEKAL, Y., MANCINI, L., ROOK, L., MEDIN TEKLE, T., TUNIZ, C. and MACCHIARELLI, R. 2014. The late Early Pleistocene human dental remains from Uadi Aalad and Mulhuli-Amo (Buia), Eritrean Danakil: macromorphology and microstructure. *Journal of Human Evolution*, **74**, 96–113.

— DEAN, C.M., ROOK, L., BONDIOLI, L., MAZURIER, A. and MACCHIARELLI, R. 2016. Enamel thickness and enamel growth in *Oreopithecus*: Combining microtomographic and histological evidence. *Comptes Rendus Palevol*, **15**, 209–226.

— KULLMER, O., KELLEY, J., BACON, A.-M., DEMETER, F., DUMONCEL, J., FIORENZA, L., GRINE, F.E., HUBLIN, J.-J., TUAN NGUYEN, A., HUONG NGUYEN, T.M., PAN, L., SCHILLINGER, B., SCHRENK, F., SKINNER, M., JI, X. and MACCHIARELLI, R. 2019. Evidence for increased hominid diversity in the Early to Middle Pleistocene of Indonesia. *Nature Ecology and Evolution*, **3**, 755–764.

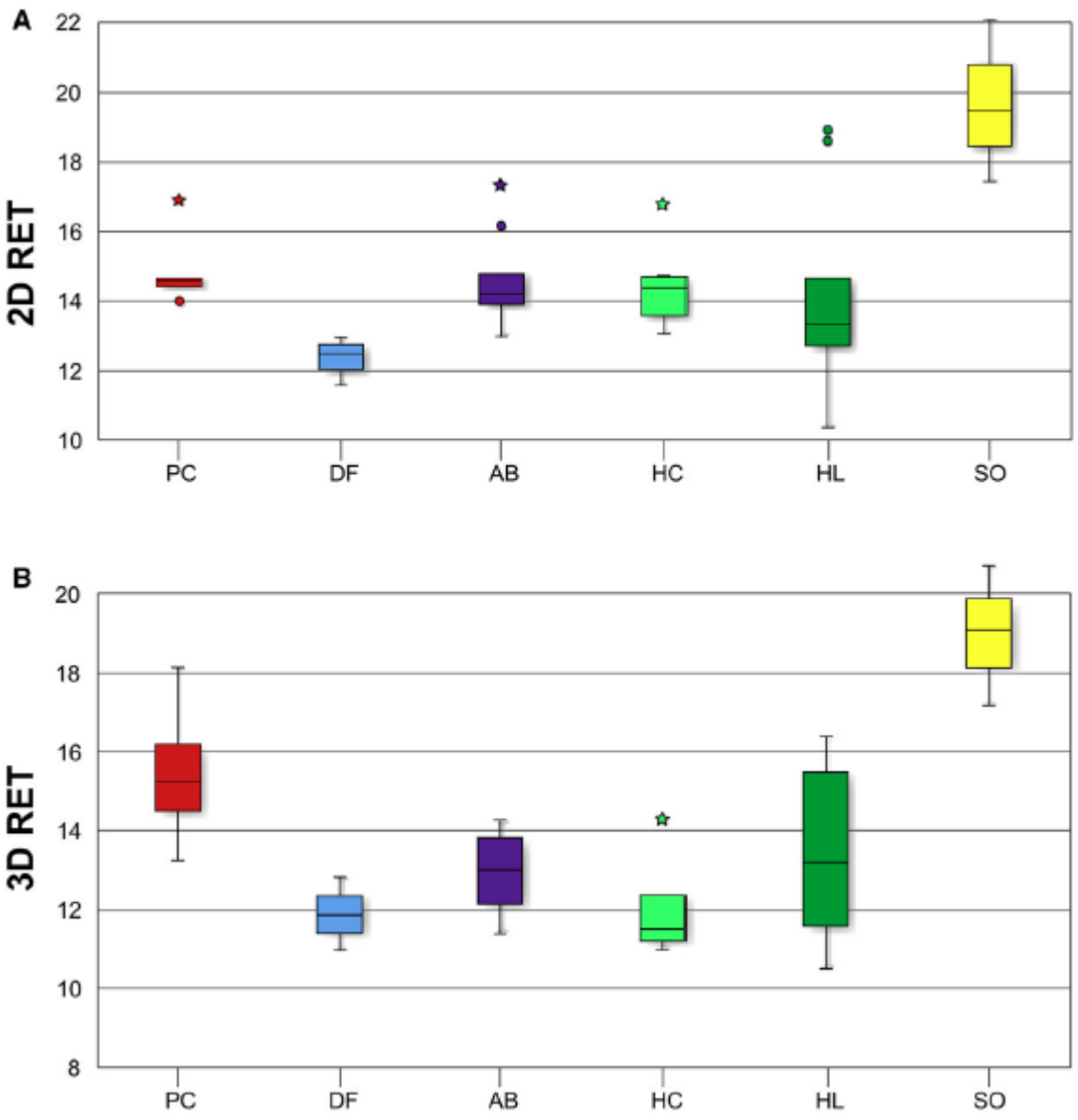

Fig. 1. Boxplots comparing relative enamel thickness among dryopithecine species recorded in NE Iberian Peninsula: (A) 2D RET; (B) 3D RET. Only taxa represented by at least three specimens are depicted. Boxes represent the interquartile range (IQR; 25th and 75th percentiles), centerline is median, whiskers denote the maximum and minimum values within 1.5 times the IQR, dots are outliers, and stars represent extreme outliers. Abbreviations: PC, *Pierolapithecus catalaunicus*; DF, *Dryopithecus fontani*; AB, *Anoiapithecus brevirostris*; HC, *Hispanopithecus crusafonti*; HL, *Hispanopithecus laietanus*; SO, "*Sivapithecus*" *occidentalis* species inquirenda.

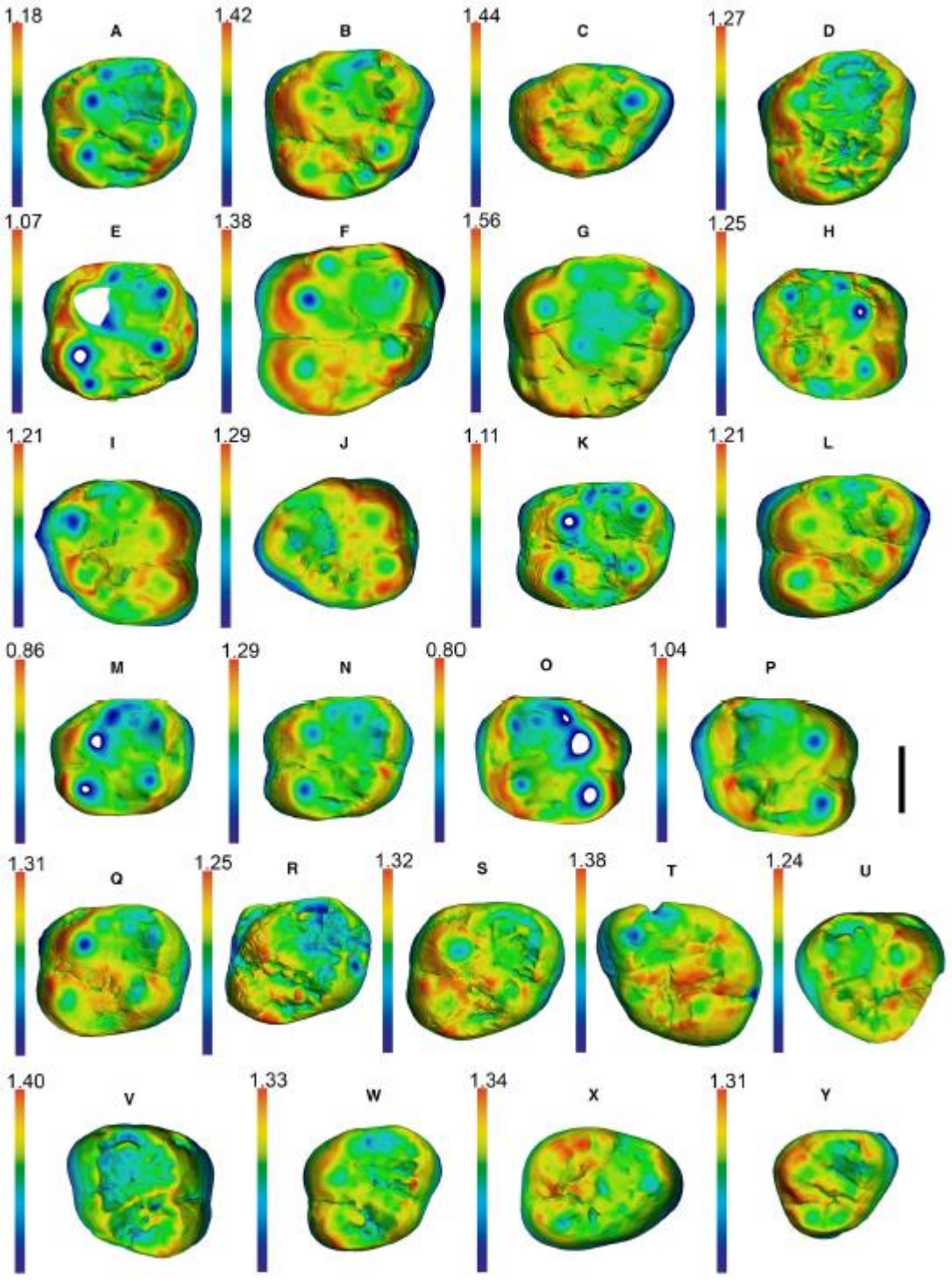

Fig. 2. Upper molar enamel distribution maps of Iberian dryopithecines. (A–C) *Pierolapithecus catalaunicus* (IPS21350, holotype): L M^1 (A), L M^2 (B), and L M^3 (C); (D) *Dryopithecus fontani* (MGSB48486): R M^2; (E–G) *D. fontani* (IPS35026): L M^1 (E), L M^2 (F) and L M^3 (G); (H–L) *Anoiapithecus brevirostris* (IPS43000, holotype): R M^1 (H), R M^2 (I), R M^3 (J), L M^1 (K) and L M^2 (L); (M–P) *A. brevirostris* (IPS35027): L M^1 (M), L M^2 (N), R M^1 (O) and R M^2 (P); (Q–U) *Hispanopithecus crusafonti* (paratypes): L M^1 IPS1818 (Q), R M^1 IPS1815 (R), L M^2 IPS1820

(S), R M^3 IPS1812 (T) and R M^3 IPS1814 (U); (V–Y) *Hispanopithecus laietanus*: R M^2 IPS1844 (V), L M^2 IPS58339 (W), L M^3 IPS58340 (X) and L M^3 IPS1772 (Y). Each tooth has its own color scale of enamel thickness, ranging from 0 to maximum thickness (indicated in mm above the scale). Scale bar represents 5 mm.

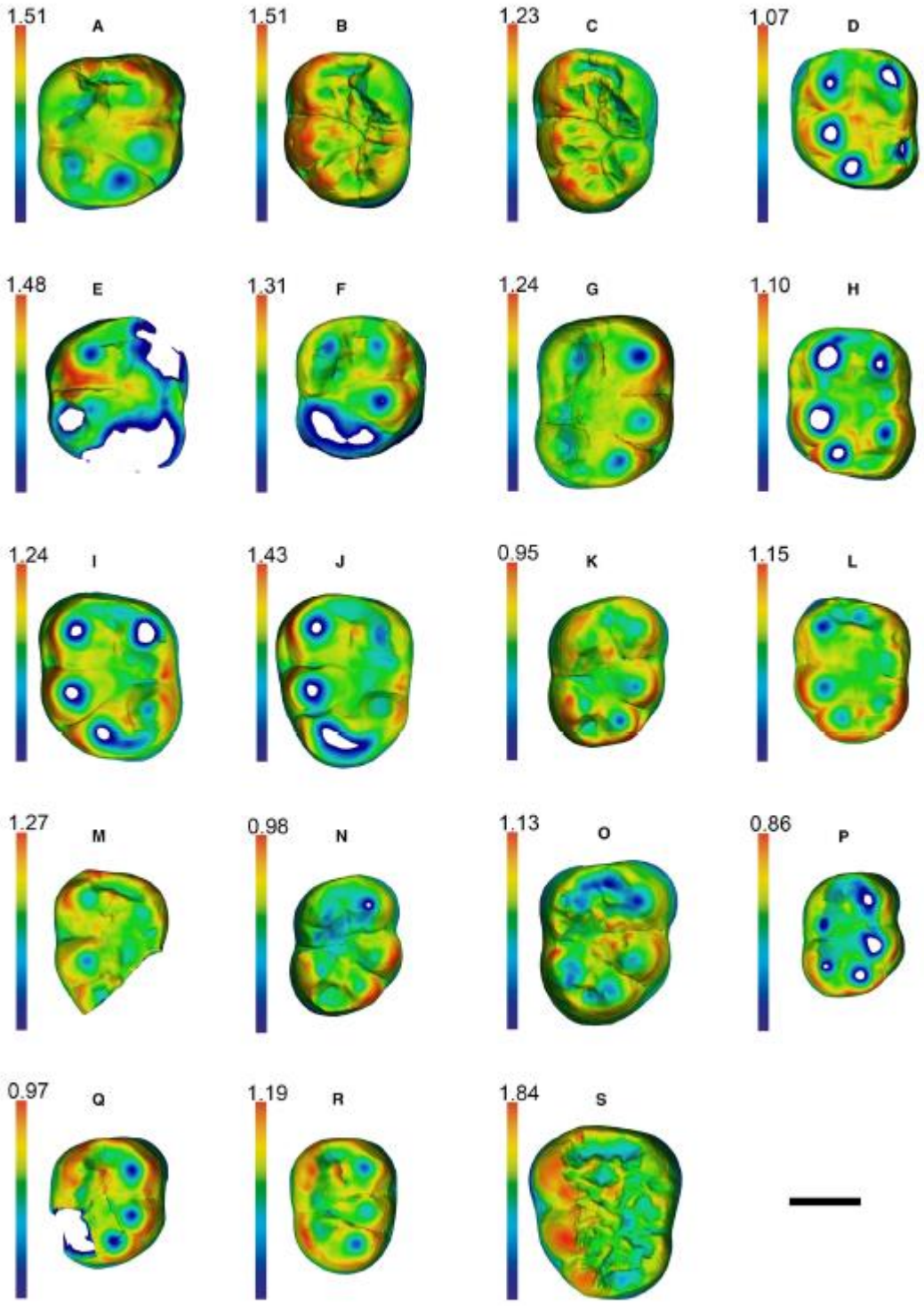

Fig. 3. Lower molar enamel distribution maps of Iberian dryopithecines. (A) "*Sivapithecus*" *occidentalis* species inquirenda (IPS41734): R M_2; (B–C) "*S.*" *occidentalis* (holotype): L M_2 IPS1826 (B) and L M_3 IPS1827 (C); (D–F) *Anoiapithecus brevirostris* (IPS43000, holotype): L M_1 (D), L M_2 (E), R M_1 (F); (G) *Hispanopithecus crusafonti* (IPS1816, paratype): R M_2; (H–J) *H. crusafonti* (MGSB25314): L M_1 (H), L M_2 (I) and L M_3 (J); (L–M) *Hispanopithecus laietanus* (IPS1804, holotype): L M_2 (L) and L M_3 (M); (K, N–S) *H. laietanus*: R M_2 IPS1780 (K), R M_1

IPS1797 (N), R M_2 IPS1797 (O), R M_1 IPS1802 (P), R M_2 IPS1802 (Q), R M_3 IPS1802 (R) and L M_3 IPS1822 (S). Each tooth has its own color scale of enamel thickness, ranging from 0 to maximum thickness (indicated in mm above the scale). Scale bar represents 5 mm.

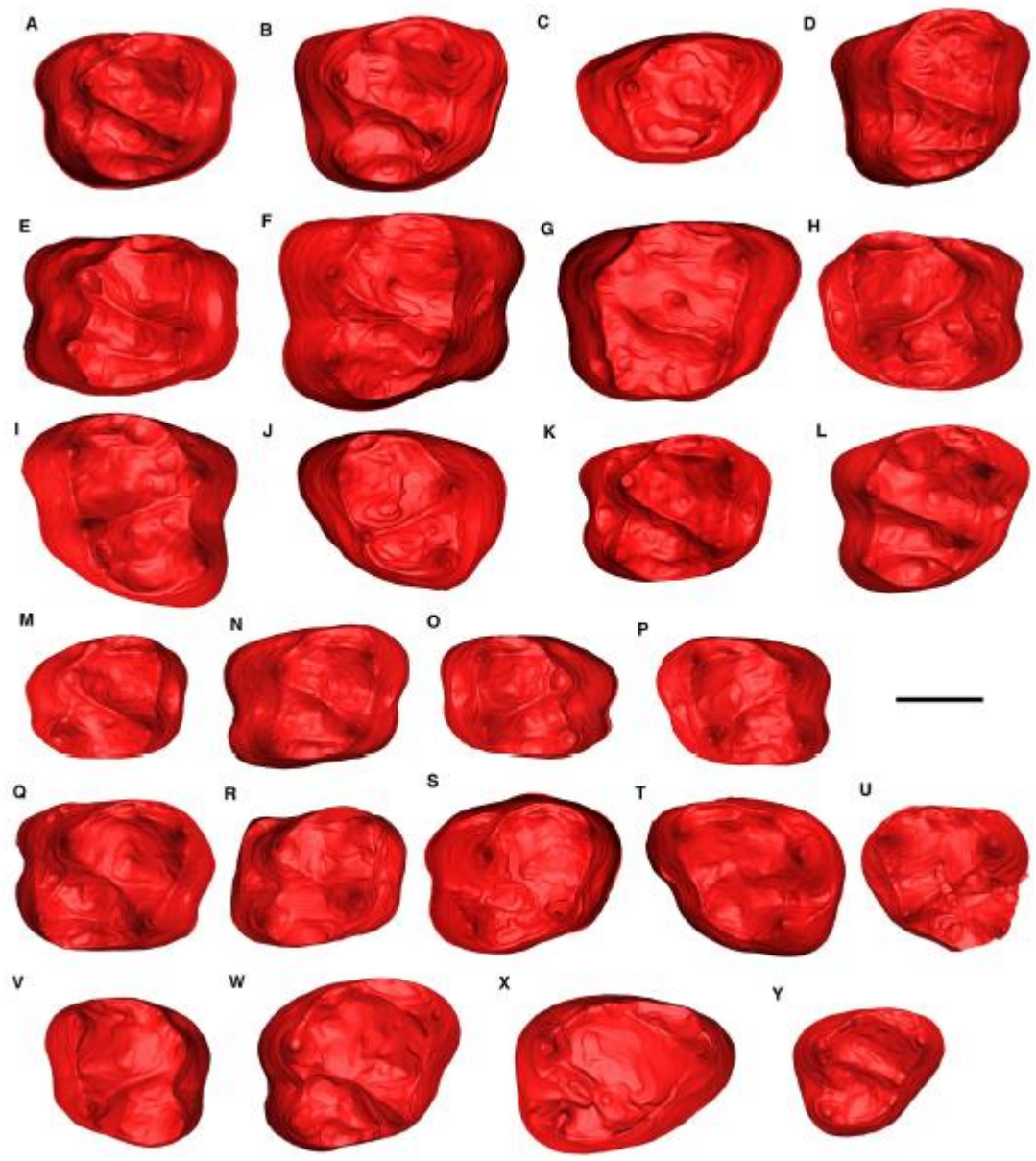

Fig. 4. Upper molar enamel-dentine junction (EDJ) Iberian dryopithecines. (A–C) *Pierolapithecus catalaunicus* (IPS21350, holotype): L M^1 (A), L M^2 (B), and L M^3 (C); (D) *Dryopithecus fontani* (MGSB48486): R M^2; (E–G) *D. fontani* (IPS35026): L M^1 (E), L M^2 (F) and L M^3 (G); (H–L) *Anoiapithecus brevirostris* (IPS43000, holotype): R M^1 (H), R M^2 (I), R M^3 (J), L M^1 (K) and L M^2 (L); (M–P) *A. brevirostris* (IPS35027): L M^1 (M), L M^2 (N), R M^1 (O) and R M^2 (P); (Q–U) *Hispanopithecus crusafonti* (paratypes): L M^1 IPS1818 (Q), R M^1 IPS1815 (R), L M^2 IPS1820 (S), R M^3 IPS1812 (T) and R M^3 IPS1814 (U); (V–Y) *Hispanopithecus laietanus*: R M^2 IPS1844 (V), L M^2 IPS58339 (W), L M^3 IPS58340 (X) and L M^3 IPS1772 (Y). Scale bar represents 5 mm.

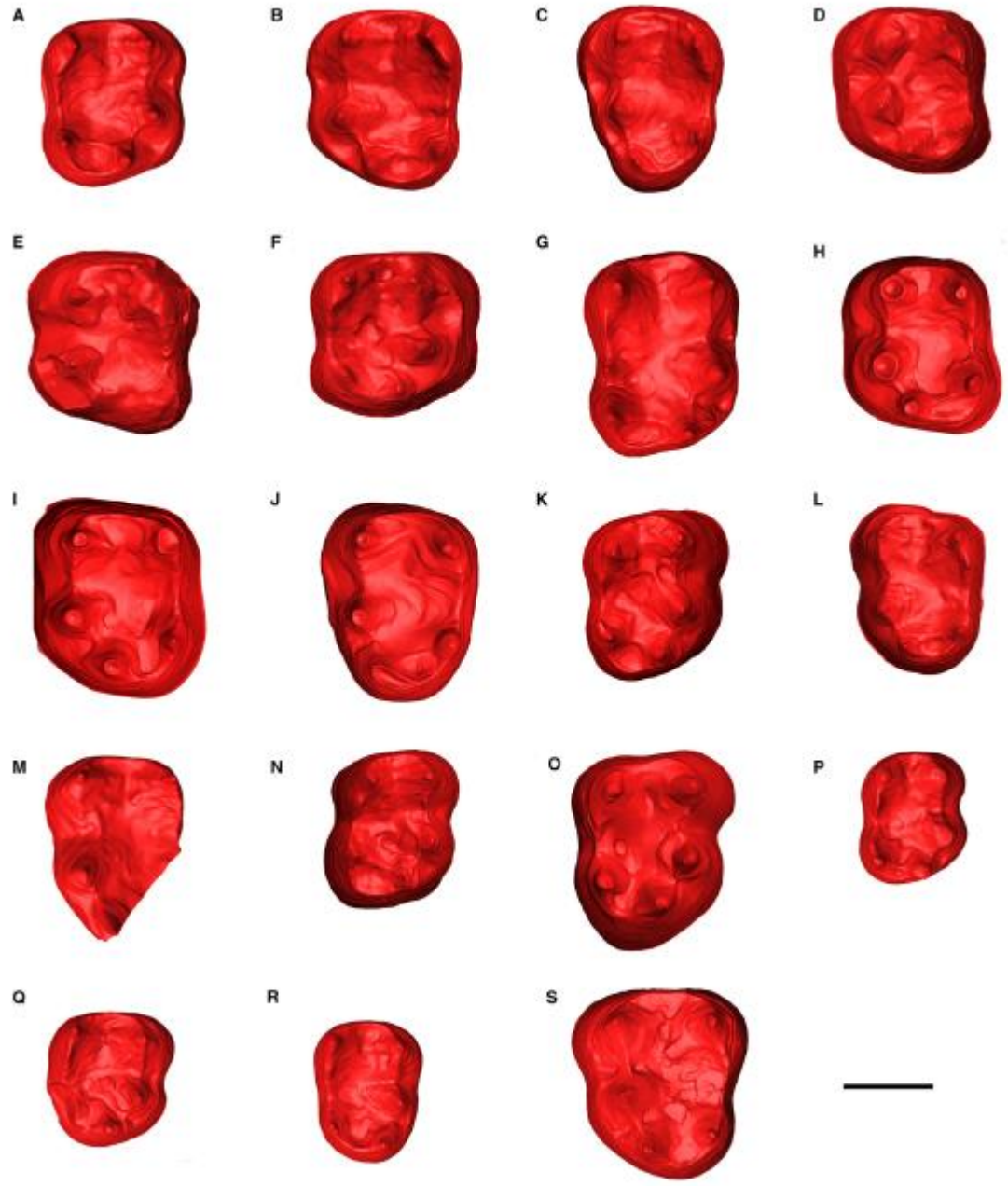

Fig. 5. Lower molar enamel-dentine junction (EDJ) of Iberian drypithecines. (A) "*Sivapithecus*" *occidentalis* species inquirenda (IPS41734): R M_2; (B–C) "*S.*" *occidentalis* (holotype): L M_2 IPS1826 (B) and L M_3 IPS1827 (C); (D–F) *Anoiapithecus brevirostris* (IPS43000, holotype): L M_1 (D), L M_2 (E), RM_1 (F); (G) *Hispanopithecus crusafonti* (IPS1816, paratype): R M_2; (H–J) *H. crusafonti* (MGSB25314): L M_1 (H), L M_2 (I) and L M_3 (J); (L–M) *Hispanopithecus laietanus* (IPS1804, holotype): L M_2 (L) and L M_3 (M); (K, N–S) *H. laietanus*: R M_2 IPS1780 (K), R M_1 IPS1797 (N), R M_2 IPS1797 (O), R M_1 IPS1802 (P), R M_2 IPS1802 (Q), R M_3 IPS1802 (R) and L M_3 IPS1822 (S). Scale bar represents 5 mm.

Table 1. Studied samples of Miocene hominoids from Catalonia.

Specimen	Tooth	Wear[1]	Locality[2]	Age (Ma)	Taxon	Remarks
IPS1772	L M^3	1–2	CLL1	9.7	*Hispanopithecus laietanus*	–
IPS1780	R M_2	1–2	CLL1	9.7	*Hispanopithecus laietanus*	–
IPS1797	R M_1	2–3	CLL1	9.7	*Hispanopithecus laietanus*	–
IPS1797	R M_2	1–2	CLL1	9.7	*Hispanopithecus laietanus*	–
IPS1802	R M_1	3	CLL1	9.7	*Hispanopithecus laietanus*	Invalid holotype of '*Rahonapithecus sabadellensis*' (nomen nudum)
IPS1802	R M_2	1–2	CLL1	9.7	*Hispanopithecus laietanus*	Invalid holotype of '*Rahonapithecus sabadellensis*' (nomen nudum)
IPS1802	R M_3	1–2	CLL1	9.7	*Hispanopithecus laietanus*	Invalid holotype of '*Rahonapithecus sabadellensis*' (nomen nudum)
IPS1804	L M_2	2	LT	9.5	*Hispanopithecus laietanus*	Holotype
IPS1804	L M_3	1–2	LT	9.5	*Hispanopithecus laietanus*	Holotype
IPS1812	R M^3	1	CP1	10.4–10.0	*Hispanopithecus crusafonti*	Paratype
IPS1814	R M^3	1–2	CP1	10.4–10.0	*Hispanopithecus crusafonti*	Paratype
IPS1815	L M^1	1–2	CP1	10.4–10.0	*Hispanopithecus crusafonti*	Paratype
IPS1816	R M_2	2	CP1	10.4–10.0	*Hispanopithecus crusafonti*	Paratype
IPS1818	L M^1	1–2	CP1	10.4–10.0	*Hispanopithecus crusafonti*	Paratype
IPS1820	L M^2	1–2	CP1	10.4–10.0	*Hispanopithecus crusafonti*	Paratype
IPS1822	L M_3	1	CLL1	9.7	*Hispanopithecus laietanus*	Invalid holotype of '*Dryopithecus piveteaui*' (nomen nudum)
IPS1826	L M_2	1	CV	12.5-11.9	'*Sivapithecus*' *occidentalis* species inquirenda	Holotype of '*Sivapithecus*' *occidentalis*
IPS1827	L M_3	1	CV	12.5-11.9	'*Sivapithecus*' *occidentalis* species inquirenda	Holotype of '*Sivapithecus*' *occidentalis*
IPS1844	R M^1	1	CLL1	9.7	*Hispanopithecus laietanus*	–
IPS18000.5	R M^1	4	CLL2	9.6	*Hispanopithecus laietanus*	–
IPS18000.5	R M^2	2	CLL2	9.6	*Hispanopithecus laietanus*	–
IPS18000.5	R M^3	1–2	CLL2	9.6	*Hispanopithecus laietanus*	–
IPS21350	L M^1	1–2	ACM/BCV1	11.9	*Pieralopithecus catalaunicus*	Holotype
IPS21350	L M^2	1–2	ACM/BCV1	11.9	*Pieralopithecus catalaunicus*	Holotype
IPS21350	L M^3	2	ACM/BCV1	11.9	*Pieralopithecus catalaunicus*	Holotype
IPS21350	R M^1	2	ACM/BCV1	11.9	*Pieralopithecus catalaunicus*	Holotype
IPS21350	R M^2	1–2	ACM/BCV1	11.9	*Pieralopithecus catalaunicus*	Holotype
IPS35026	L M^1	3	ACM/C3-Ae	11.9	*Dryopithecus fontani*	–
IPS35026	L M^2	2	ACM/C3-Ae	11.9	*Dryopithecus fontani*	–
IPS35026	L M^3	1–2	ACM/C3-Ae	11.9	*Dryopithecus fontani*	–
IPS35027	R M^1	3	ACM/C1-E*	12.3–12.2	*Anoiapithecus brevirostris*	–
IPS35027	R M^2	1–2	ACM/C1-E*	12.3–12.2	*Anoiapithecus brevirostris*	–
IPS35027	L M^1	3	ACM/C1-E*	12.3–12.2	*Anoiapithecus brevirostris*	–
IPS35027	L M^2	1–2	ACM/C1-E*	12.3–12.2	*Anoiapithecus brevirostris*	–
IPS41734	R M_2	1	ACM/BCV4	11.9	'*Sivapithecus*' *occidentalis* species inquirenda	–
IPS43000	R M^1	1	ACM/C3-Aj	11.9	*Anoiapithecus brevirostris*	Holotype
IPS43000	R M^2	1–2	ACM/C3-Aj	11.9	*Anoiapithecus brevirostris*	Holotype
IPS43000	R M^3	1	ACM/C3-Aj	11.9	*Anoiapithecus brevirostris*	Holotype
IPS43000	L M^1	2	ACM/C3-Aj	11.9	*Anoiapithecus brevirostris*	Holotype
IPS43000	L M^2	1–2	ACM/C3-Aj	11.9	*Anoiapithecus brevirostris*	Holotype
IPS43000	L M_1	3	ACM/C3-Aj	11.9	*Anoiapithecus brevirostris*	Holotype
IPS43000	L M_2	4	ACM/C3-Aj	11.9	*Anoiapithecus brevirostris*	Holotype
IPS43000	R M_1	3	ACM/C3-Aj	11.9	*Anoiapithecus brevirostris*	Holotype
IPS58339	L M^2	1	CLL1	9.7	*Hispanopithecus laietanus*	Probably same individual as IPS58340
IPS58340	L M^3	1	CLL1	9.7	*Hispanopithecus laietanus*	Probably same individual as IPS58339
MGSB48486	R M^2	1	HP	12.5–9.7	*Dryopithecus fontani*	–
MGSB25314	L M_1	4	TF	10.4–10.0	*Hispanopithecus crusafonti*	–
MGSB25314	L M_2	3–4	TF	10.4–10.0	*Hispanopithecus crusafonti*	–
MGSB25314	L M_3	3	TF	10.4–10.0	*Hispanopithecus crusafonti*	–

Abbreviations: **Specimen**: IPS, 'Institut de Paleontologia de Sabadell', former name of Institut Català de Paleontologia Miquel Crusafont; MGSB, Museu de Geologia del Seminari de Barcelona; **Tooth**: L, left; R, right; **Locality**: ACM, local stratigraphic series of Abocador de Can Mata (els Hostalets de Pierola); C1, Cell 1 (ACM sector); C3, Cell 3 (ACM sector); BCV, Barranc de Can Vila (ACM sector); CLL, Can Llobateres (Sabadell); CP, Can Poncic (Sant Quirze); CV, Can Vila (els Hostalets de Pierola); HP, Hostalets de Pierola indet. (els Hostalets de Pierola); LT, La Tarumba; TF, Teuleria del Firal (Seu d'Urgell).

[1]Wear stages are adapted from Smith (1984).

[2]Numerals after locality abbreviations refer to stratigraphic levels within a single site; other alphanumeric combinations after ACM sectors (separated by a dash) refer to subsectors.

Table 2. Descriptive statistics for relative enamel thickness.

Taxon (localities)[1]	N	MNI	Mean	2D RET					
				SD	SE	95% CI	95% CI	Minimum	Maximum
Pierolapithecus catalaunicus (ACM/BCV1)	5	1	15.36	1.15	0.51	14.35	16.37	13.99	16.88
Dryopithecus fontani (ACM/C3-Ae, HP)	3	2	12.33	0.71	0.41	10.56	14.10	11.55	12.95
Anoiapithecus brevirostris (ACM/C3-Aj, ACM/C1-E*)	9	2	14.58	1.35	0.45	13.70	15.46	12.97	17.32
Hispanopithecus crusafonti (CP1, TF)	7	3	14.39	1.26	0.48	13.46	15.33	13.03	16.76
Hispanopithecus laietanus (CLL1, CLL2, LT)[2]	17	5	14.34	2.77	0.67	13.02	15.66	10.35	19.11
'*Sivapithecus*' *occidentalis* (ACM/CV, ACM/BCV4)	3	2	19.66	2.35	1.36	17.01	22.32	17.43	22.11
Taxon (localities)[1]	N	MNI	Mean	3D RET					
				SD	SE	95% CI	95% CI	Minimum	Maximum
Pierolapithecus catalaunicus (ACM/BCV1)	4	1	15.46	2.03	1.02	13.47	17.45	13.24	18.14
Dryopithecus fontani (ACM/C3-Ae, HP)	3	2	11.87	0.93	0.54	10.83	12.92	10.96	12.81
Anoiapithecus brevirostris (ACM/C3-Aj, ACM/C1-E*)	7	2	12.93	1.11	0.42	12.11	13.75	11.40	14.26
Hispanopithecus crusafonti (CP1, TF)	4	2	12.06	1.51	0.76	10.58	13.53	10.97	14.27
Hispanopithecus laietanus (CLL1, CLL2, LT)	10	3	13.46	2.18	0.69	12.11	14.82	10.49	16.38
'*Sivapithecus*' *occidentalis* (ACM/CV)	3	2	18.96	1.74	1.00	16.99	20.92	17.16	20.63

Abbreviations: MNI, minimum number of individuals; SD, standard deviation; SE, standard error; CI, confidence interval; **Locality**: ACM, local stratigraphic series of Abocador de Can Mata (els Hostalets de Pierola); C1, Cell 1 (ACM sector); C3, Cell 3 (ACM sector); BCV, Barranc de Can Vila (ACM sector); CLL, Can Llobateres (Sabadell); CP, Can Poncic (Sant Quirze); CV, Can Vila (els Hostalets de Pierola); HP, Hostalets de Pierola indet. (els Hostalets de Pierola); LT, La Tarumba; TF, Teuleria del Firal (Seu d'Urgell).

[1]Numerals after locality abbreviations refer to stratigraphic levels within a single site; other alphanumeric combinations after ACM sectors (separated by a dash) refer to subsectors.

[2]*H. laietanus* specimens include histological sections from Andrews & Martin (1991) and Kelley *et al.* (2001) as reported by Smith *et al.* (2019).

Table 3. Qualitative dental features of the EDJ of the upper molars.

Features	*Pierolapithecus catalaunicus*	*Dryopithecus fontani*	*Anoiapithecus brevirostris*	*Hispanopithecus crusafonti*	*Hispanopithecus laietanus*
Dentine horns	Slightly peripheral	Slightly peripheral	Slightly to moderately peripheral	Moderately peripheral	Very peripheral
Mesial fovea	Shallow and moderately developed	Shallow and mesially located	Deep and restricted	Deep and restricted	Shallow and restricted
Trigon basin	Deeper	Shallower	Deeper	Deeper	Shallower
Crista obliqua	High, complete and straight	Moderately high and centrally twisted	High, complete and straight	Low and often disrupted	Moderately high and often disrupted
M^1–M^2 hypocone	Aligned with or slightly more lingual than protocone	Markedly more lingual than protocone only in M^1	Markedly more lingual than protocone	Markedly more lingual than protocone	Aligned with or slightly more lingual than protocone
Buccolingual waisting	Slight	Moderate	Marked	Variable (slight to moderate)	Variable (slight to moderate)
Lingual cingulum	Slightly developed	Moderately developed	Well developed	Well developed	Slightly developed

Table 4. Qualitative dental features of the EDJ of the lower molars.

Features	*Hispanopithecus crusafonti*	*Hispanopithecus laietanus*	'*Sivapithecus*' *occidentalis*
Metaconid horn	Vertical	Vertical	Tip centrally tilted
Protoconid and entoconid horns	Variable but generally peripheral	Variable but generally peripheral	Less peripheral
Buccal cingulid	Well developed	Absent to poorly developed	Well developed
Lower molar crown waisting	Slight	Marked	Moderate
Tuberculum intermedium (interconulid)	Sometimes present	Absent	Variable
M^2 metaconulid (twinned metaconid)	Absent	Rarely expressed	Marked
Hypoprotocristid and hypometacristid	Nearly indistinct and interrupted	Nearly indistinct and interrupted	Marked, although not merged